NEOTECTONIC STUDY OF GANGA AND YAMUNA TEAR FAULTS, NW HIMALAYA, USING REMOTE SENSING AND GIS

A thesis submitted
in partial requirements
for the degree of

MASTER OF TECHNOLOGY

by

PRADEEP KUMAR SAHOO

to the
DEPARTMENT OF CIVIL ENGINEERING
INDIAN INSTITUTE OF TECHNOLOGY, KANPUR
June, 1997

CE-1997-M-SAH-NEO

CERTIFICATE

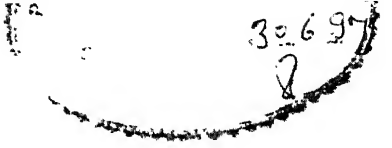

Certified that the work presented in this thesis entitled **"NEOTECTONIC STUDY OF GANGA AND YAMUNA TEAR FAULTS, NW HIMALAYA, USING REMOTE SENSING AND GIS"** has been carried out by **Sri Pradeep Kumar Sahoo** (Roll No. 9510330) under my supervision and has not been submitted elsewhere for a degree.

RP Singh 30/6/97

Ramesh P. Singh
Professor
Department of Civil Engineering
Indian Institute of Technology
Kanpur - 208 016

ABSTRACT

Ganga and Yamuna rivers emerge from Himalaya along two major faults known as Ganga and Yamuna Tear Faults, respectively. The two major strike-slip faults transverse to the Siwalik range are clearly seen in satellite imagery of Dehradun area. Earthquake records, landslide and recent changes in geomorphological features indicate that the area between Main Boundary Thrust (MBT) and Main Frontal Thrust (MFT) is tectonically active. An effort has been made to study the tectonic evolution and neotectonism of Ganga and Yamuna tear faults. Both spectral and spatial enhancement techniques have been employed to the digital data of IRS-1B LISS-I to delineate the lineaments and major faults of the area. Based on Mohr's theory failure criteria and statistical analysis of remotely sensed lineament data, the horizontal compressive stress ($S_{H\max}$) has been estimated at various sites of the study area. These data are consistent with the published $S_{H\max}$ orientation determined from earthquake focal mechanism solution. With help of a computer program active faults and lineaments have been extracted from the previously obtained remotely sensed lineament data. The past earthquake data and basement depth contour data have been used to have an integrated approach with the help of available GIS techniques to reconstruct present day regional geodynamic model. Attempts have been made to investigate the genesis of Ganga and Yamuna tear faults and possible cause of recent tectonic activities of the area with the help of proposed geodynamic model.

ACKNOWLEDGMENTS

I take this opportunity to express my deep sense of gratitude to Dr. Ramesh P. Singh for the constant inspiration, support and encouragement given to me, not only during the course of this thesis, but also at other critical times of my M. Tech. program. His exemplary guidance, commendable patience and clear deep insight into problems benefited me immensely in completing this work.

I thank gratefully to Dr. V. K. Gahalaut, Department of Earth Sciences, University of Roorkee, Roorkee, for the earthquake data provided by him. I am also thankful to Sandeep Kumar for his sincere help during the thesis work.

I acknowledge the help received from Umesh Singh, Saroj Panda, Asim Chatterjee, Vikrant Jain, Ajay Srivastav, Arun, Tanmaya, Aditya, Patel and all other members of Engineering Geology laboratory in doing this thesis.

Finally, I am thankful to the All India Council For Technical Education, New Delhi for the financial support through sponsored research project to Dr. R.P. Singh.

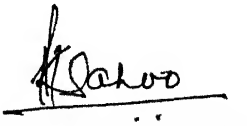

PRADEEP KUMAR SAHOO

CONTENTS

LIST OF FIGURES

LIST OF TABLES

LIST OF ABBREVIATIONS

MCT : Main Central Thrust

MBT : Main Boundary Thrust

MFT : Main Frontal Thrust

HFT : Himalayan Foothill Thrust

IGP : Indo-Gangetic Plain

IGF : Indo-Gangetic Foredeep

GTF : Ganga Tear Fault

YTF : Yamuna Tear Fault

DHR : Delhi Hardwar Ridge

DIP : Digital Image Processing

GIS : Geographic Information System

CHAPTER I

INTRODUCTION

1.0 GENERAL

Since time immemorial man has undergone innumerable ordeals due to its casual approach towards nature. The remote sensing technology has proved to be very potential tool in solving many hidden mysteries about the Earth. Yet, we have not been able to understand all the processes related to our planet Earth. Numerous earthquakes of higher and lower magnitudes in Himalayan region have posed many challenges to our ultra modern technology. With increasing demand of energy and need of space to accommodate our bursting population, the Himalayan region has caught the eyes of the people. Numbers of hydel projects have been recently planned in this mountainous terrain and as a result few townships have been grown. However, the fate of all these man made structures obviously owe its legacy to the devastating Nature. So before further expansion of modern civilization on the foothills and along the hill flanks it is necessary to go by the old common saying "prevention is better than cure".

Evolution of the Himalayas from deep Tethys to mountain ranges has gone through a number of face lift since Quaternary age. First the Indus - Tsangpo suture zone then the successive southward high tectonic zones i.e. Main Central Thrust (MCT), Main Boundary Thrust (MBT) and Main Frontal Thrust (MFT) are becoming more devastation prone regions. The presence of transverse lineaments and faults as Ganga and Yamuna tear faults in the above mentioned tectonic zones are receiving attention of many Earth scientists. A number of scientific works have been commenced to understand the exact structure and neotectonic activities associated with these transverse lineaments. The recognition of structural kinematics units to get a seismic classification of a region the first

step in the analysis of seismic hazards. Such units are domains that can be considered as homogeneous for the deformative and kinematics and seismic sources.

Satellite remote sensing has emerged as powerful tool for Earth scientists in geological investigation of inaccessible regions. The synoptic overview of a wide area and digital nature of the remote sensing data can be utilized suitably to map the active tectonic features. Digital image processing of IRS data can be utilized to enhancement of spectral gray levels or subtle tonal variations, such as those caused by lithological changes, geological structures, etc. The remote sensing imageries emphasize linear features, fractures or faults that can be difficult to map in conventional methods of mapping, particularly in Himalayan terrain. Appropriate statistical analysis of remotely sensed faults, lineaments and other structural elements, allow the separation of tectonic phases and computation of stress condition in a region. Routine use of remote sensing data and its analysis of a hazard prone area, help in monitoring the changes in surficial/geomorphological features. Based on such changes, occurrence of a natural hazards can be predicted or a mega project in such areas can be avoided which can save lives and properties.

The modern Geographic Information System (GIS) has been recently used by Earth scientists in multi-disciplinary geological investigations. Using GIS, attempts have been made to study a phenomena from various angle, using several approaches and as many attributes as possible or considered reasonable, to obtain a more comprehensive and clearer picture. The role of integrated strategy in neotectonic study involving remote sensing, geological data, micro-earthquake data and other related data from different sources is being increasingly appreciated. The integrated multi-disciplinary approach helps to understand the regional geodynamic processes and their surficial structural impressions of a region.

1.1 SCOPE AND OBJECTIVE OF THE WORK

In the present study, the area around Dehradun lying between the latitude 29.52^0 - 31.18^0 N and longitude 76.89^0 - 78.55^0 E (Figure 1.1), NW Himalaya, has been chosen for application of satellite data and geographic information system, in the study of neotectonism. The area shown in the image (Figure 1.2) is a part of active tectonic zone of Indian and Eurasian plate collision. An improvement of thematic cartography is necessary because of the high seismicity which may affects this area having relatively high population density. The area has experienced recent tectonic activities. Devastating earthquakes like Kangra (1905) and Uttarkashi (1991) in near by areas are the manifestation of recent earth movements or stress deformations. An analysis of the catalogue of past earthquakes have revealed that these earthquakes are not isolated events, but only the latest expression of diffuse seismic activities.

The vastness, wildness and rugged morphology of the area which was studied makes the use of satellite images indispensable. The integrated use of remote sensing data with extensive field checks allows the reconstruction of pattern of deformation with a good degree of precision. Quantitative statistical analysis of deformational features like lineaments and faults provides some of the valuable clues to separate out active tectonic zones. Special attention has been paid to understand the origin and neotectonism of transverse lineaments, particularly the Ganga and Yamuna tear faults. Integration of historical micro-earthquakes data, geological, basement topography data and remote sensing data gives useful elements for neotectonic and geodynamic evaluation of the whole region, which is the overall objective of present study.

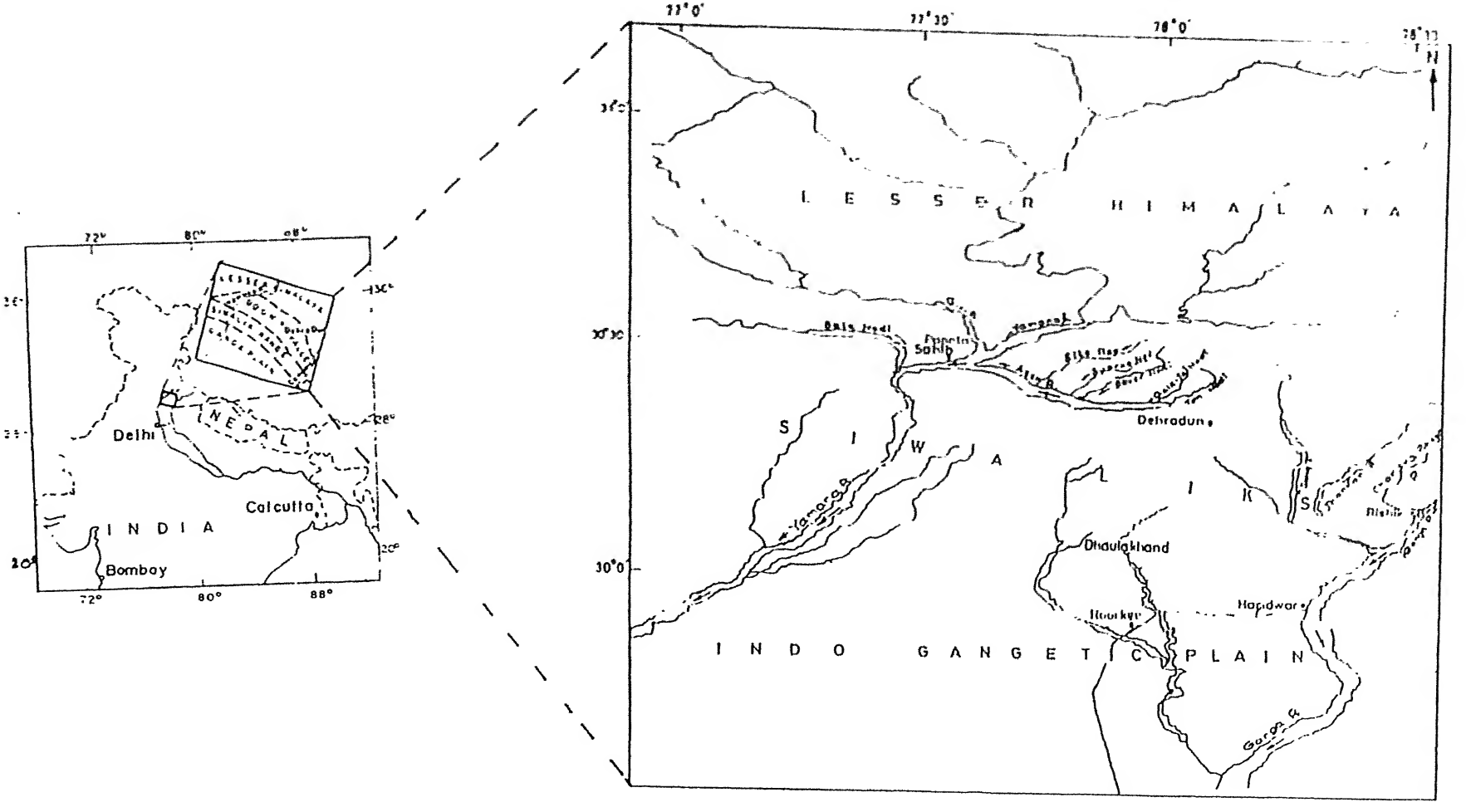

Figure 1.1 Location map of the study area

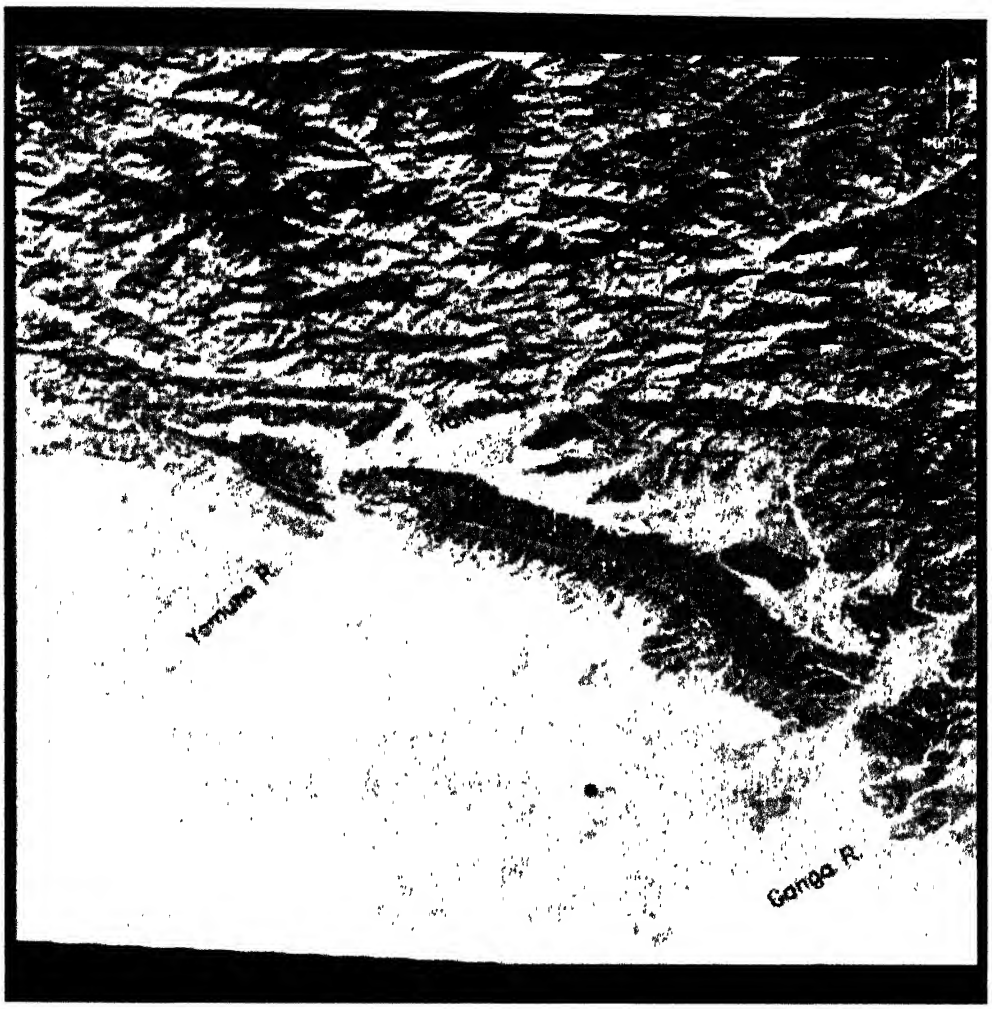

Figure 1.2 IRS-1B LISS -I image (FCC of Band 4,2,1) of the study area

1.2 ORGANISATION OF THE WORK

The present study in this thesis is presented in five chapters. Chapter I deals with the introduction, scope and objective of the work. Chapter II includes geological framework and seismicity of the study area. Chapter III gives a general outline about the scope of satellite remote sensing and geographical information system in natural hazard assessment and mitigation. In chapter IV, we have given details of digital image processing techniques to enhance lineaments and faults in images and statistical analysis and application of remotely sensed lineament fabric data. An integrated approach has been made in this chapter, using GIS and digital image processing result to reconstruct the regional present day geodynamic model and neotectonism of the study area. The summary and conclusions of the work have been presented in chapter V.

CHAPTER II

GEOLOGICAL FRAMEWORK AND SEISMICITY OF THE AREA

2.0 GENERAL

The study area can be broadly divided into four physiographical zones (Figure 2.1) - the Indo-Gangetic Plain, Siwalik Range, Lesser Himalayan Range and the Dun Valley. The four zones are characterized by different types of lithology.

2.1 GEOLOGICAL FRAMEWORK

2.1.1 Indo-Gangetic Plain:

The plain in the southern most extremity is covered by thick quaternary alluvium and recent soils. The alluvium is highly fertile and has been extensively used for agriculture.

2.1.2 Siwalik Range:

The narrow elongated Tertiary sandstone sequence of Siwalik range is exposed towards north. The contact boundary between the Siwalik and Indo-Gangetic alluvium deposit, regionally called as Main Frontal Thrust (MFT) or more simply as Himalayan Foothill Thrust (HFT). The structural hills of Siwalik are highly dissected, with rugged topography and densely vegetated.

The Siwalik Group represents one of the thickest fluviatile sequences of the world (Opdkyke et al., 1982). Basically rocks of Middle and Upper Siwalik are exposed in the area. The Lower Siwalik rocks are believed to be covered by the alluvium of Indo-Gangetic Plain in the south. The whole Siwalik sequence consists of about 6000 m thick inter bedded mudstone, sandstone, conglomerate and subordinate marls, deposited in a complex channel fan and braided river system. The middle Siwalik succession contains fine to medium grain relatively matured sediments whereas

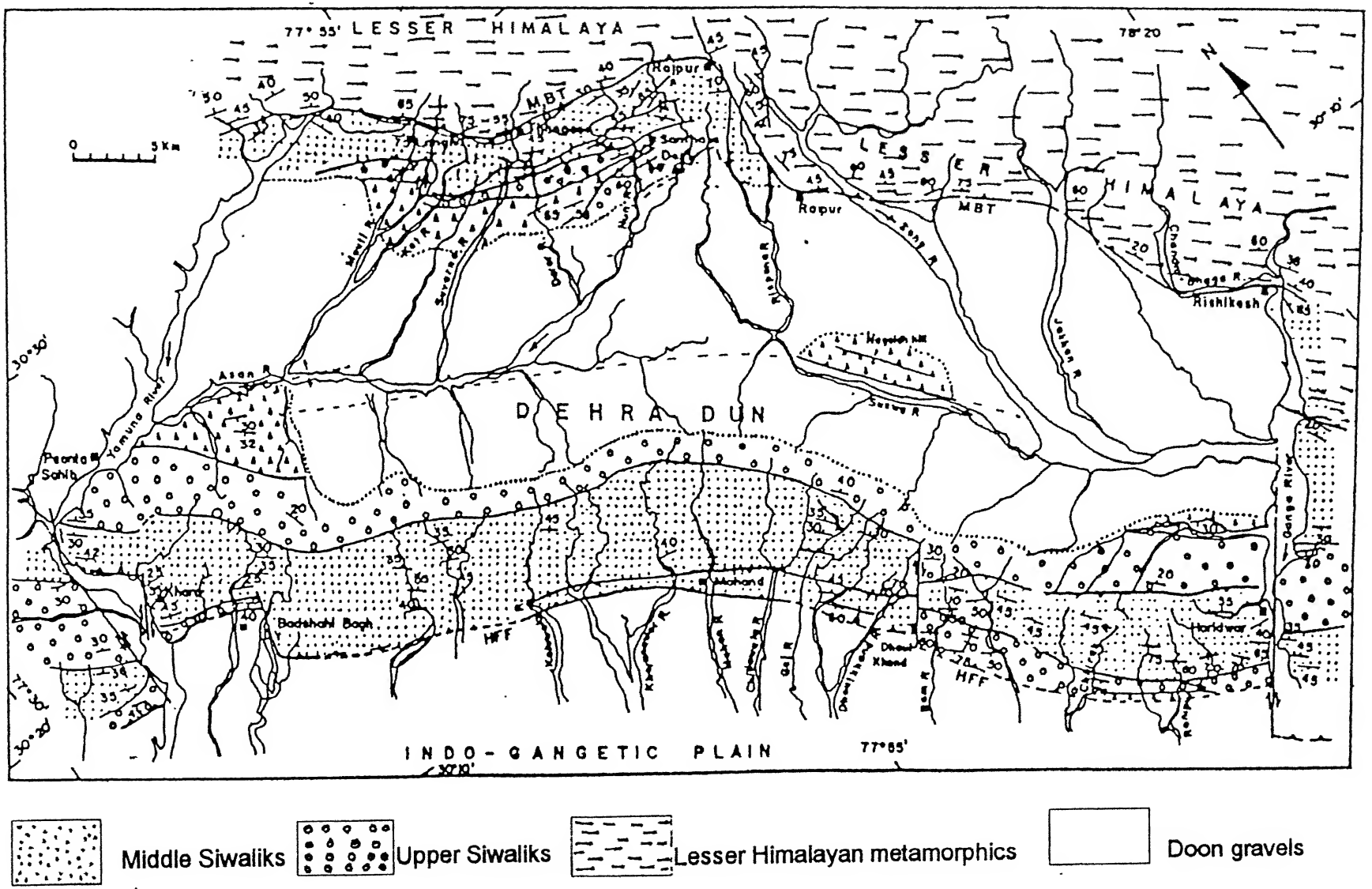

Figure 2.1 Geological map of the area (modified after Rautela and Sati, 1996)

the Upper Siwalik comprises of loose coarse grained sandstone, boulders and conglomerate. With the rapid upliftment of the Himalayan mountain in succeeding tectonic impulses, the sediments deposited in Upper Siwalik succession acquired increasingly coarse and immature characters.

The east-west continuity of the Siwalik range has broken by two transverse tear faults. These faults are well marked in the satellite imagery. Though these are not exposed, presumed to run along the coarse of Ganga and Yamuna rivers and well known as Ganga and Yamuna Tear Faults, respectively. Besides numerous small faults, joints, lineaments, anticlinal folds are the striking features of the Siwalik range.

2.1.3 Dun Valley:

Dun valley lies between Ganga and Yamuna rivers in the east and west, respectively. It is a longitudinal synclinal valley bounded by Siwalik and Lesser Himalayan range and forms a part of the sub-Himalayan foothill zone. The valley is mainly covered by Dun gravels and recent alluvium. The Dun gravels are characteristically composed of sub-angular to sub-rounded unconsolidated heterogeneous mixture of clastic quartzite, limestone, shales, phyllite, granite, gneiss, schist, basic rocks etc., in a matrix of silt, clay and sand (Philip, 1996). This sediments have been mostly derived by the streams flowing from the lesser Himalayan metamorphics and Siwalik sedimentary sequence. Dun gravels are of post Siwalik age and are involved in the folding movement (Philip, 1996).

2.1.1 Lesser Himalayan Range:

The entire northern part of the area is covered by the Lesser Himalayan mountain ranges. The area comprised mainly of pre-Tertiary sedimentary and meta-sedimentary rocks which have been subjected to low degree of metamorphism. The rocks are grouped in Blaini-Krol-Tal of Mussoorie Group (Valdiya, 1980). The Lesser Himalayan meta-sediments tectonically overrides Siwaliks and Dun gravels at places, by Main Boundary Thrust (MBT). This is a highly deformed, lithologically and

structurally complex terrain. This area is traversed by numerous faults and shear zones along which low grade metamorphism has taken place. Folds, faults, joints, slickenside striations and fault breccia are the common structural features of the lesser Himalayan rocks.

2.2 GENERALISED STRATIGRAPHIC SUCCESSION OF THE AREA

The stratigraphy of the area is well established. Geology of the area is highly complicated because of the complex interplay of tectonic and stratigraphic elements. In fact this region represents a part of Siwalik - Lesser Himalayan complex. The generalised stratigraphic succession of the area is given in the table 2.1.

2.3. NEOTECTONIC HISTORY AND STRUCTURAL EVOLUTION OF THE AREA

The Himalayan mountain chain is an unique and classical example of continental collision (Qureshy et al., 1992). Geodynamic evolution of the Himalayas has been modeled into a global framework of the under thrusting Indian plate underneath the Eurasian plate along the Indus-Tsangpo suture zone. The continuous horizontal compression of Indian plate against Tibet was responsible for the building of the continental crust by stacking a series of north dipping thrust flakes like mid-Tertiary MCT, MBT and the late Tertiary MFT from north to south (Figure 2.1). As a result of this crustal shortening, the lesser Himalayan Proterozoic foreland is thrusted over by gneissose and schistose metamorphic piles of the Higher Himalaya along MCT. The whole succession is found to be thrusted southward over the Cenozoic foredeep molasses deposits of Siwaliks along MBT. After a transitionary succession, the widespread middle Miocene - Pleistocene Siwalik Group of clastic fluviatile sediments, was deposited in an east-west elongated basin, a forerunner of the Indo-Gangetic Plain. The sedimentary fill within the basin represents large mega-cone similar to those forming at present in the Indo-Gangetic plain. Due to collision of

Table 2.1. Generalised Stratigraphic Succession

Age	Formations	Rock types
Sub Recent - Recent	Alluvium Dun gravels	
//////////////////////////////////	////////////////MFT//////////////	//////////////////////////////////
Middle Miocene - Pleistocene	Upper	coarse boulder conglomerates, clays, sandstones, grits
	SIWALIK — Middle	Massive sandstone, clays, pebbly at the top
	Lower	Dark hard sandstone, purple shale
Eocene	Subathu Bed	Gray, green, maroon shale, Quartzite, Limestone.
//////////////////////////////////	////////////////MBT//////////////	//////////////////////////////////
Jurassic	Tal formation	Thick Quartzite, Greywackes, Chert bands, Shale etc.
Permian	Krol Formation	Limestone and Shale
Carboniferous	Infra-Krol Formation	Dark gray bleached Shale.
	Blaini Bed	Cream colored limestone and Boulder bed
Devonian	Nagthat	Sandstone, Quartzite, Grits, Conglomerate, Clay stones.
	Chandpur	Quartzite, Schist, Phyllite.
Cambrian	Mandhali	Slate, limestone, Boulder beds

(modified succession after CCIL)

Indian and Eurasian plates, the northern edge was fragmented by dip-slip normal fault to produce the foreland basin which received sediments from the uplifted provinces of the main Himalaya. Starting from Higher Himalaya in the source region, more southerly areas have been successively raised and subsequently eroded off with time during the deposition of the Siwalik Group. These acted as a significant additional source for the Siwalik sediments in the latter part of their sediment history.

The Indo-Gangetic Foredeep (IGF) sediments occur in a number of sub-basins separated from each other by transverse sub-surface tectonic features in the thrust contact (MFT) with the deformed Siwalik sediments of the Himalaya (Qureshy et al., 1992).

2.4. SEISMICITY AND NEOTECTONISM

The micro-earthquake data during 1720 to 1995 show that the Himalaya is a young region of deformation where tectonic motion and earthquakes are very active. The continuous horizontal compression of Indian plate against Tibetan plate, following collision, leads to the accumulation of strain which at times is released along the MCT, MBT, and MFT and is consistent with focal mechanism solution of earthquakes as an intraplate deformation (Qureshy et al., 1989). This continuous compression put the Himalaya under a continuous state of strain and has significant bearing in neotectonism. The devastating earthquakes such as the 1897 event (Ms - 8.7) over Shilong plateau, 1905 in Kangra region (Ms - 8.6), 1934 in Bihar (Ms - 8.4), the 1950 event along Mishmi thrust region in Assam and the 1991 event in Uttarkashi (Ms - 7.0) are some of the recent manifestations due to tectonic activities in the region. Major events that have taken place along the Himalayan arc are shown in figure 2.2. An interesting feature of the seismicity of the Himalaya is that large magnitude earthquakes have also taken place in area south of the MBF. These includes the 1827, 1832 and 1851 events near Lahore (Punjab plain), the 1720 earthquake near Delhi and 1803 earthquake near Mathura.

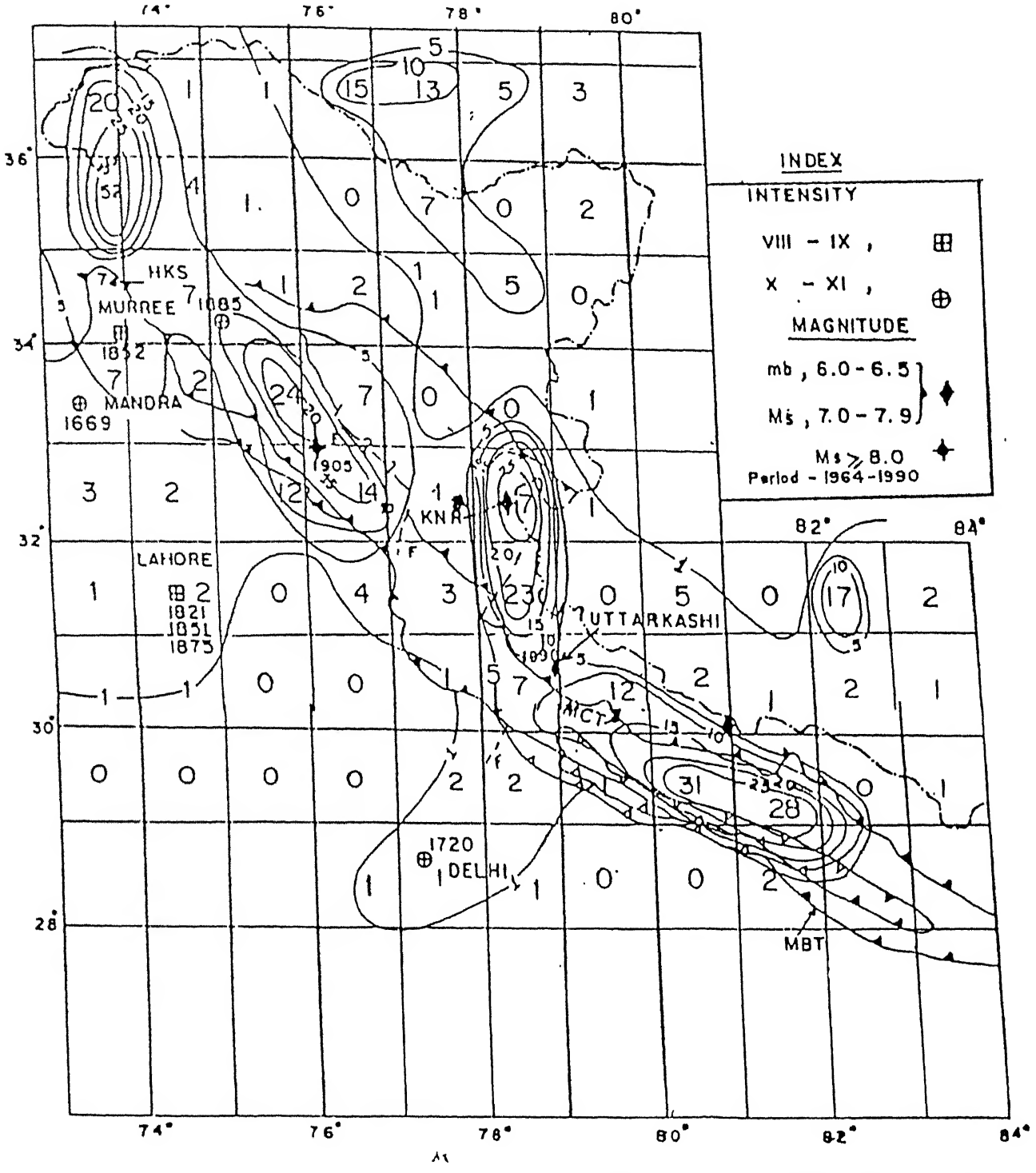

Figure 2.2 The figure shows relative seismicity of different regions of NW Himalaya, for the period of (1964 - 1990) based on N, magnitude ≥ 4.5. Delhi-Hardwar ridge and Kinnaur region are the major transverse features (after Verma et. al., 1995)

The Bizarre earthquake of 1934 (Ms - 8.4) has also taken place 50 - 60 km south of MBF. Numerous minor tremors have also been reported in IGF and Siwalik regions.

Verma et al. (1972) have prepared A and b value maps based on the following relationship:

$$\log N = A - b*M$$

where, N represents the cumulative number of events of magnitude greater than or equal to M, and A and b are constants which are different for different regions.

Figure 2.2 shows the relative seismicity of different regions of NW Himalaya based on N, mag > 4.5 for $1^0 \times 1^0$ area. This figure brings out following interesting features regarding the tectonism of NW Himalaya, which are given below (Verma et al., 1995):

(1) Punjab/Kashmir Himalaya (32^0 -35^0 N, 75^0 - 77^0 E), the area which are seismically most active at present lie to the NW of the region where the 1905 Kangra earthquake took place. The contours here are NW - SE trend in conformity with that of the Himalayan thrusts (MBT, MCT).

(2) Kinnaur region (31^0 - 35.5^0 N, 78^0 - 79^0 E) is well defined N-S trending seismic region. In this region, the seismicity has been explained in terms of faults created due to a pull apart structure, which have been created very recently as a result of collision of the Indian plate with Tibet (Ni and Bazarngi, 1985).

(3) Garhwal - Kumaun Himalaya region is seismically very active which lie between 28^0 to 30.5^0 N, 82^0 to 90^0E. The contours have a NW-SE trend in conformity with

that of Himalayan thrusts. Uttarkashi earthquake of October 1991 has taken place in a small gap between Kinnaur and Kumaun-Himalaya.

(4) The contours bring out the broad structure of Delhi-Hardwar Ridge (DHR).

2.4.1. Seismicity of NW Himalaya

Figure 2.3 shows seismic events having magnitude, mb>4.0 (for the period of 1720-1995) occurred in NW Himalaya and close to MBF. Figure 2.3 shows that the events are not strictly close to the MBF. Several historical events having intensity VII and above are also shown. It is noticed that several areas south of MBF show appreciable seismicity. These include DHR, Mathura-Muradabad fault, where historical events of 1920 (intensity VIII) and 1803 have been reported (Verma et al., 1991).

2.4.2 Transverse Lineaments and Recent tectonic activities

Several transverse lineaments are seismically active in the region. These include DHR and Kinnaur lineament, delineated by the geophysical and seismic data. The DHR constitutes a very prominent feature located between 28^0 to 30^0 N and 76^0 to 79^0 E, having a NE-SW trend (Verma et al., 1995). Several recent earthquakes of magnitude 5.0 or above have been reported along this basement ridge.

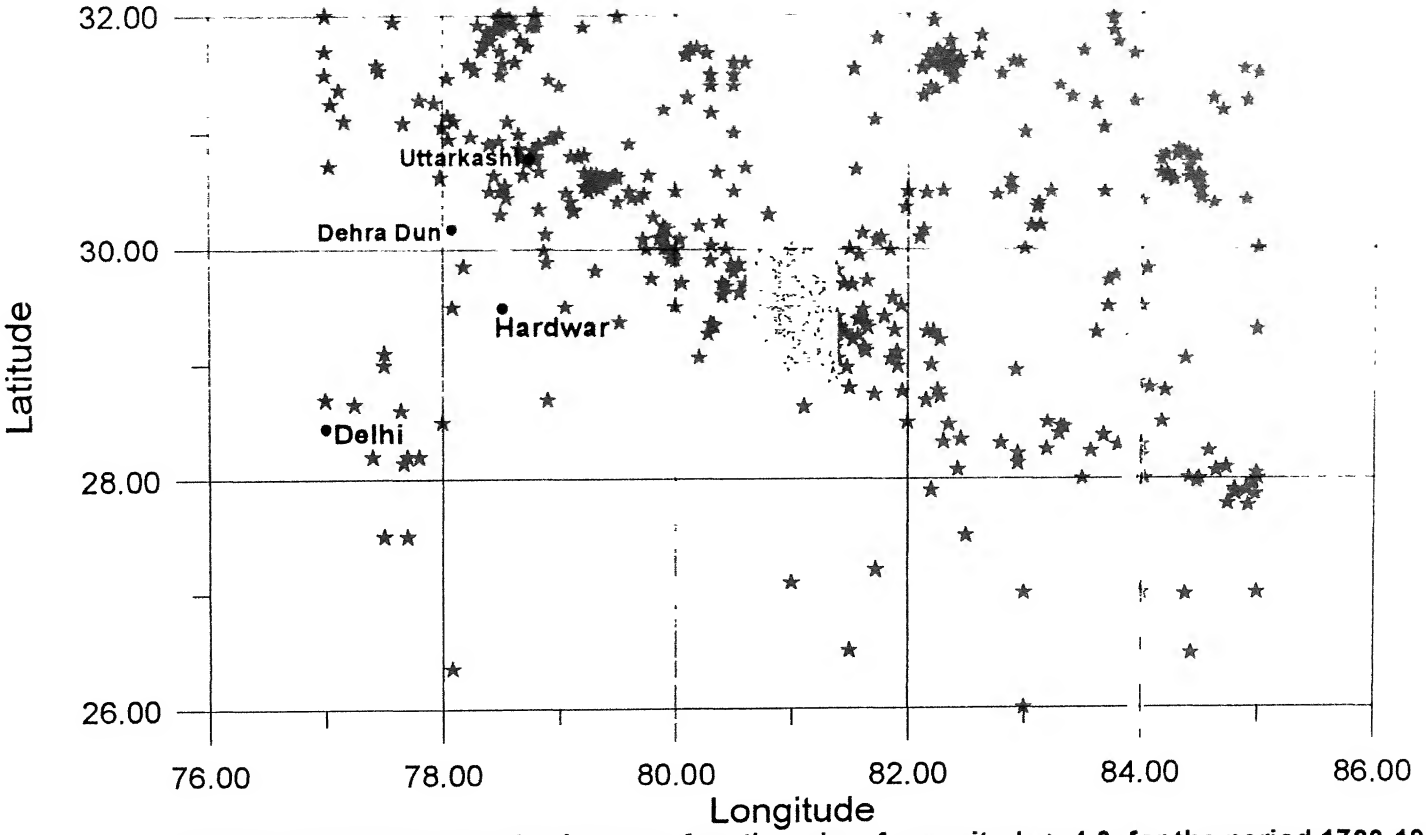

Figure 2.3 Distribution of epicenter of earthquake of magnitude ≥ 4.0, for the period 1720-1995

CHAPTER III

NATURAL HAZARDS AND REMOTE SENSING

3.0 GENERAL

Natural hazards such as earthquakes, volcanoes, forest fire, landslides, subsidence, storms and floods are natural phenomena which occur every year in some part of the world. Due to these natural hazards loss of life and damage to the property occur. Efforts have been made to monitor these natural hazards for their firmly prediction locally and at regional scale. Recently, use of remote sensing technique has been explored for natural hazard assessment and mitigation and efforts have been made to use this technique in proper monitoring of natural hazards. All types of remotely sensed data are being employed for this purpose. Remote sensing technique are being used in all three aspects of disaster management vulnerability assessment, warning and damage assessment. In order to explore these issues, however, it is necessary to understand the underlying causes of natural disasters and the relevant technical capabilities of the satellite systems. The rapid growth in the number and effectiveness of earth observation satellite presents a wide range of new capabilities which can be used to mitigate the effect of disasters or even to avoid them altogether.

3.1 APPLICATION OF REMOTE SENSING TO DISASTER MANAGEMENT

A natural disaster is the result of occurrence of a natural phenomenon (a hazard) with which a population can not deal thus resulting in mortality, injury, displacement and economic loss. Several considerations underlie this simple definition. Most important is the ability to deal with disasters. In general, we can not control Nature and we can not stop the natural calamities result from these hazards. We can, however, control man's

relationship to Nature, we can control our exposure to hazards, we can try to avoid disasters, and we can try to alleviate the effects of a disaster should one occur.

Table 3.1 Examples of the uses of space remote sensing in disaster management

	PREVENTION	PREPAREDNESS (WARNING)	RELIEF
EARTHQUAKE	Mapping geological lineaments and landuse	Geodynamic measurements of strain accumulation	*Locate stricken areas, map damage*
VOLCANIC ERUPTION	**Topographic** and landuse map	**Detection/measurements of gaseous emissions**	Mapping lava flows, ash falls and lahars, map damage
LANDSLIDES	**Topographic** and landuse map	**Soil porosity, rainfall, slope stability**	*Mapping landslide area*
FLASH FLOODS	Landuse maps	Local rainfall measurements	*Map flood damage*
MAJOR FLOODS	Flood plain maps, landuse maps	Regional rainfall, evapotranspiration	Map extent of damage
STORM SURGES	Landuse and land cover maps	Sea state, ocean surface wind velocities	*Map extent of damage*
HURRICANES		**Synoptic weather forecasts**	*Map extent of damage*
TORNADOES		Nowcasts, local weather observations	*Map amount, extent of damage*
DROUGHT		**long-ranged climate models**	Monitoring vegetative biomass, station communications

Normal - operational or needs very little research
Underlined - Research and development required
Bold - requires improved observation capacity
Italics - Requires improved spatial and temporal resolution

(after Walter, 1994)

Example of the uses of remote sensing in three aspects of disaster management is presented in table 3.1. In this table, a distinction is made among applications which are currently operational, those requiring improved observing systems and those requiring specifically, ultra high spatial or temporal resolution. In the present work, special attention has been paid to seismic hazard assessment.

3.2 NEOTECTONISM AND SEISMIC HAZARD ESTIMATION

Earthquake causes great misery and extensive damage every year. The technology of actual earthquake prediction to save people and resources are still in infancy. Seismic risk analysis deals with estimating the likelihood of seismic hazard and damage in a region and is based on mainly monitoring crustal deformation in recent time, fault morphology and measuring fault displacement. Indirect evidences based on geomorphological features, paleoseismicity and local ground conditions. Remote sensing can provide valuable inputs to these aspects.

3.2.1 Fault Morphology and Monitoring Crustal Deformation

One of the principal uses of remote sensing has been the mapping of the regional geological structures. The ability to look at texture over a wide area, and to distinguish different lithological units, have allowed investigation of ancient and current crustal deformation.

Remote sensing has been employed routinely in geological research to map faults and other aspects of geology. Vertical to high angle fault or suspected faults can be easily delineated from the remote sensing data. These are indicated on the image by one of the following criteria (Gupta, 1991, Murphy, 1994):

(1) Image lineation which may or may not be straight.

(2) Displacement and truncation of beds or key horizons.

(3) Drag effects.

(4) Presence of scarps and triangular facets.

(5) Major fault is also indicated by major change in topography.

(6) Off setting of streams

(7) Alignment of springs, streams, vegetation.

(8) Straight segment of a stream, waterfall across a stream, knick points, local steepening of stream gradient and disruption of channels and valley.

(9) Active faults are defined on the basis of displacement of some of the recent phenomena such as housing, road, rivers or recent sediments.

(10) Active faults will often show a scatter of seismic activity on or around the fault trace.

Low-angle faults are difficult to interpret, since the images provide planar views from the above such faults have strongly curving or irregular outcrop and can be inferred on the basis of discordance between the rock types, e.g. in attitude of beds, degree of deformation and degree of metamorphism, etc.

Figure 3.1 shows some of the major Cenozoic and post-Cenozoic faults delineated from the satellite imagery of Dehra Dun area. Three major zones of strike slip faulting have been mapped in this belt oriented along the river Yamuna, Dhaulakhand and Ganga with lateral shift of about 30 km, 3 km and 20 km, respectively. In the core of Dun syncline an east-west trending thrust has been identified along the south border of the Nagsiddh hill situated to the south of Rajpur (Routela and Sati, 1996). This is a shallow north dipping thrust plane between anticlinal upper Siwalik and Holocene gravel (Figure 3.1). The fault is not exposed towards the Yamuna but an anticlinal structure delineated along the Asan river is indicative of its blind nature. In Dehradun city itself, prominent NW-SE (310°-130°) oriented fractures are observed in a large number of houses in a residential colony along river Rispana and these fractures are continuously opening up (Routela and Sati, 1996). Neotectonic deformation is also reported in the Dhaulkhand strike slip fault zone along Gajrao (Routela and Sati, 1996). Neotectonic adjustment of rocks here has shown to be responsible for the upliftment of the river bed.

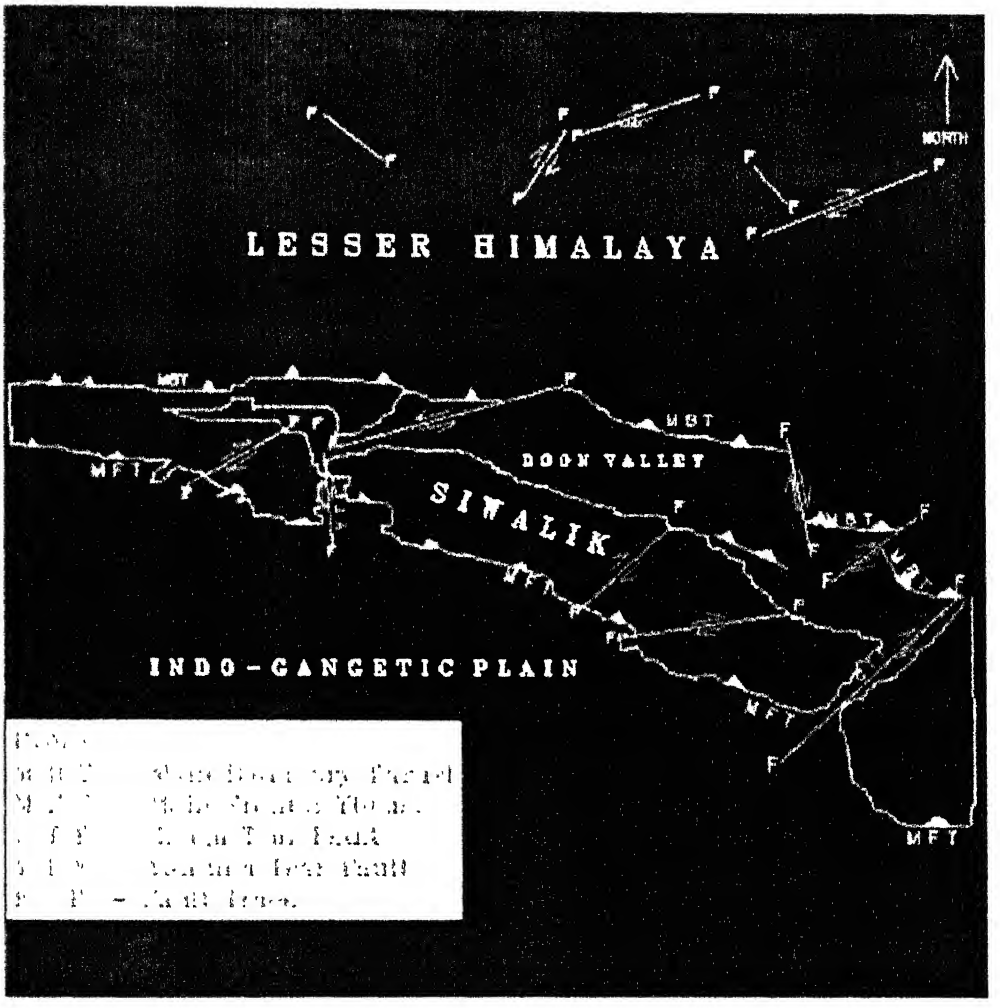

Figure 3.1 Tectonic Map Prepared From IRS-1B LISS-I Data

Geodetic studies during 1974-75 to 1978-79 and 1985 have revealed the neotectonically active nature of the Ganga tear fault (Roy and Hasija, 1995). The horizontal movement ranges from 1 to 5 cm during the period of 1974-75 to 1978-79 has been noticed. The result shown in the Figure 3.2, which exhibits a generally southward movement of the area east of the fault line. The vertical downward movement of the eastern side of the fault during the period 1974-75 to 1985 has been found to be of the order of 2 to 3 cm (Figure 3.3). This is a very significant movement and may be responsible for the active landslides in the Hardwar region. This can be taken as one of the vital precursors of an impending earthquake.

Two faults are prominent in the eastern part of the area, one along the Jhakan Rao and other towards the west of it. Due to these faults the Lesser Himalayan sequence along with MBT is disrupted. Other prominent faults are also shown in the Figure 3.1.

3.2.3 Indirect Evidence Based On Geomorphological Features

Mapping of the present day morphological features can provide important, though indirect, clues for delineating neotectonism. Peculiar patterns, for example, bending and off-setting of streams, ridges, sag ponds, springs, scarps, hanging and headless valleys, river capture etc., and their alignment in certain direction, can indicate recent movements. These features may be relatively difficult to decipher in the field, and more readily observed on remote sensing imageries, due to their planar synoptic overviews.

The drainage pattern map of the area based on satellite imagery is shown in figure 3.4. There is a marked change in drainage pattern between Lesser Himalayan and Siwalik range. In the Lesser Himalayan region, both the main streams and its tributaries displayed in right-angled bends, giving "rectangular drainage pattern". They reflect control exerted by joint or faults system (Thornbury, 1989). Two major drainage system of the Ganga and the Yamuna river are present in the Siwalik range of the study area.

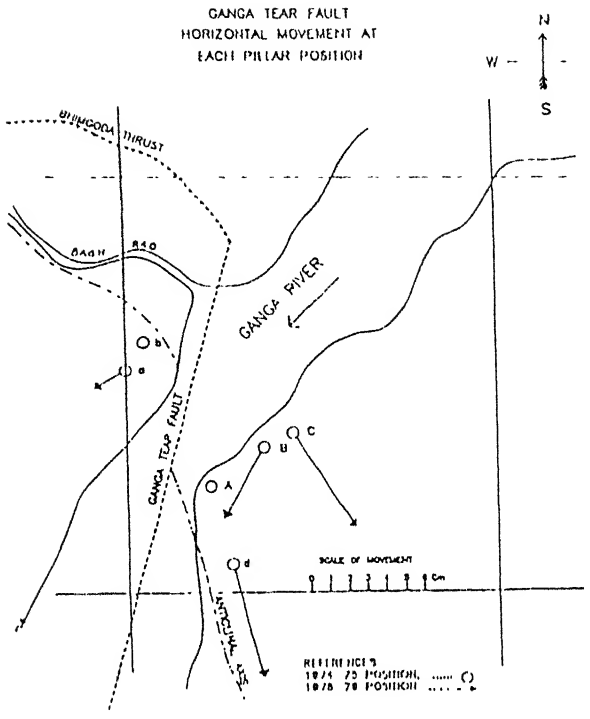

Figure 3.2 Ganga Tear Fault. Horizontal movement at each pillar position (after Roy and Hasija, 1995)

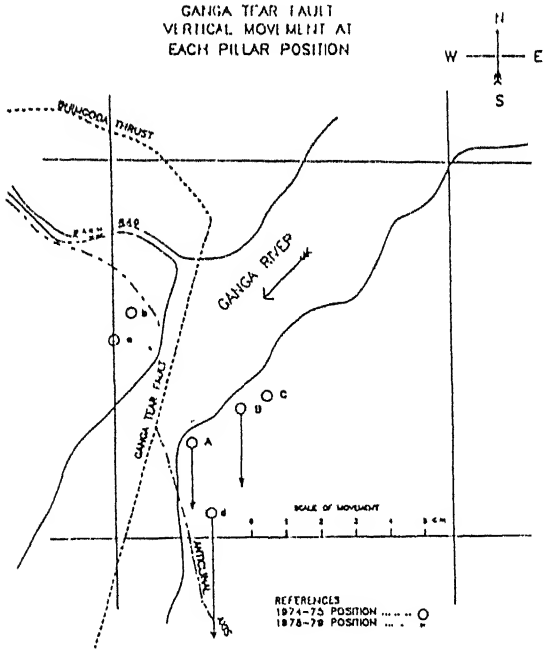

Figure 3.3 Ganga Tear Fault. Vertical movement at each pillar position (after Roy and Hasija, 1995)

The tributaries of both the river are oriented parallel or near parallel fashion, giving a typical "parallel drainage pattern". Parallel pattern are usually found where there are pronounced slope or structural controls, which lead regular spacing of parallel or near parallel streams (Thornbury, 1989).

A close analysis of drainage pattern and stream course of the region, provide some valuable information in structural interpretation of the area. The "rectangular drainage pattern" of Lesser Himalayan range in the north and "parallel drainage pattern" of Siwalik range are separated from each other by well known Main Boundary Thrust (MBT). In the Siwalik range the Ganga and Yamuna river and their tributaries have a common north-east trend. The Dhaulakhand fault (Figure 3.1) act as a drainage divide between the Ganga and the Yamuna drainage system. There is a sudden bending (more than 90°) of Bata river and Giri river meeting the Yamuna river (Figure 3.4). These are controlled by a fault along the Yamuna river, trending north-east from Paonta Sahib (Figure 3.1), which may be considered as the northward extension of the Yamuna tear fault. The abrupt end of Siwaliks along this line also indicate the presence of a fault. It extends upto the MBT and disrupts the Lesser Himalayan metamorphics.

The shift direction of major river is shown by open arrows in figure 3.4. From paleochannels and river terraces the migration direction of major rivers have been marked. The migratory trend of the river Yamuna towards west is substantiated by the abandoned channels. On the other hand the river Ganga has consistently migrated towards east (Phillips, 1994). Other small rivers like those in the Dun valley are highly entrenched in nature. These are indicating the upliftment of Dun valley in recent past.

Fig. 3.4 Drainage pattern map of the area based on IRS-1B LISS-I image.

3.2.4 Paleoseismicity

Earthquake epicenter records of past earthquakes are the further evidences of neotectonism. It can be carefully and judiciously interpreted in conjunction with data on the structural-tectonic control to derive useful information (Gupta 1991). Figures. 2.3 and 2.4 show the paleoseismicity of the NW Himalayan region between 74 to 86^{o}N and 24 to 36^{o}E. The study area lies over NNE - SSW trending DHR which is seismically active. The area has witnessed several devastating earthquakes e.g. Kangra 1905, Uttarkashi 1991, etc. in recent past. These data confirm the presence of tectonic movement in the region.

Basically remote sensing technique gives a synoptic overview of a wide area, which is very helpful for mapping regional structural, lithological and geomorphological features of recent past. These features reflect the tectonic condition and support in the assessment of natural hazards and for their mitigation.

CHAPTER IV

MAPPING OF LINEAMENTS AND STRESS ESTIMATION

4.0 GENERAL

With the introduction of satellite remote sensing technique, there has been a major upsurge of interest among the Earth scientists for investigation of various geological phenomena. Satellite image provides a synoptic view of a wide area which helps in regional geological interpretation. Digital image processing techniques have been applied to enhance various interesting geological features. Satellite images indeed have brought out many large and small scale lineaments. Applying suitable digital image processing technique, lineaments have been enhanced and mapped to study the regional geofabric of the area. Appropriate statistical treatment of geofabric data coupled with historical earthquake data may prove to be a valuable tool for neotectonic study as well as for developing geodynamic model of the area.

4.1 LINEAMENTS

Hobbe in 1904 has introduced the term lineament to define a "significant line of landscape which reveal the hidden architecture of rock basement". O' Leary et al. (1976) have defined lineament in geomorphological sense as a "mappable simple or composite linear feature of a surface, whose parts are aligned in a rectilinear or slightly curvilinear relationship and which differs distinctly from the patterns of adjacent features and presumably reflects a sub-surface phenomenon". The term lineament is used in many different ways in geosciences. Recently, a simple generalized definition of lineament has been accepted in Regional Geophysical Lineament conference at Bangalore (1989) which is given below:

"A lineament is a regional scale linear or curvilinear feature, pattern or change of pattern that can be identified in a data set and attributed to a geologic formation or structure".

Specialized lineaments such as remote sensing lineaments are accordingly redefined by inserting "remote sensing" before the "data set". The adjective "regional" in the above definition depends on the size of the area under investigation and do not refer to a specific length. Lineaments include all structural alignments, topographical alignments, natural vegetation linear and lithological boundaries etc., which are very likely to be the surface expression of the buried structure. Linear features in an imagery are attributed to the alignment of different geological features such as (Gupta, 1991):

i) Shear zones / faults

ii) Rift valleys

iii) Truncation of outcrops

iv) Fold axial traces

v) Joints and fracture traces

vi) Alignment of fissures, pipes, dykes, plutons

vii) Linear trend due to lithological layering

viii) Lines of significant sedimentary facies change

ix) Alignment of streams and valleys

x) Topographical alignment - subsidence and ridges

xii) Alignment of oil and gas fields

xiii) Occurrence of geysers, fumeroles and springs along a line

xiv) Linear features seen on gravity, magnetic and other geophysical data

xv) Vegetation alignment

xvi) Soil tonal changes etc.

xvii) Natural limits of distribution of certain earth surface features.

The manifestation of a lineament depends on the scale of observation and dimension involved. Lineaments of a certain dimension and character may be more clear on particular scale, for which reason tectonic features of the size of hundred kilometers need to be studied on smaller scale images. On certain images both major and minor lineaments are invariably observed. The major lineaments correspond to important shear zones, faults, rift valleys and major tectonic structure or boundaries. On the other hand, minor lineaments or micro-lineaments correspond to relatively minor faults, joints, fractures, bedding traces etc. These are expressed as soil tonal changes, vegetation alignment, springs, gaps in ridges, alignment of surface sags and depressions etc., and impart the textural character in a large scale.

4.2 REMOTE SENSING DATA USED IN THE PRESENT STUDY

The digital remote sensing data of IRS-1B LISS-I have been used in the present study. This data has been acquired from NRSA, Hyderabad. The specifications of the data used are given in Table 4.1.

Table 4.1 Specification of the remote sensing data

Production identification code	95\1968-03-1
Date of product generation	09-19-1995
Satellite	IRS-1B
Sensor	L1
Path-Row	29-46
Date of pass	20-OCT-94
Scene center time	11-15-09
Input scene center latitude (degrees)	30.38411713
Input scene center longitude (degrees)	77.77865601
Correction level	L2
Inter pixel distance (meters)	72
Inter line distance (meters)	72
Band interleaving indicator	BIL
Product is generated on	IBM PC/AT Compatible with MSDOS
Band numbers	1, 2, 3, 4
Record length of volume directory file	360 Bytes
Record length of leader file	3960
Record length of imagery file	2520

ERDAS (Earth Resource Data Analysis System) digital image processing PC based system has been used to display the images, and for detailed processing and analysis of remote sensing data. Apart from ERDAS, MAPINFO and IDRISI. packages have been used in the present study. These packages are being used widely by various agencies around the globe for the analysis of satellite data and their applications in geology, forestry, soil, agriculture, environmental, etc.

The multi-band digital data of Dehra Dun area having 2500 rows and 2350 columns have been used for detailed analysis. The whole scene is divided into nineteen windows of size 512 rows and 512 columns for detailed investigation of small scale features. Various image processing techniques have been used to enhance the images. Details of image processing techniques and their results have been discussed in section 4.3.

4.3 DIGITAL IMAGE PROCESSING AND LINEAMENT MAPPING

Digital Image Processing (DIP) involves the manipulation and interpretation of digital images with the aid of computer. The digital image fed into a computer one pixel at time. The computer is programmed to insert these data into an equation, or series of equations, and then store the result of computation for each pixel. These results from new digital image that may be displayed or recorded on pictorial format or may itself be further manipulated by additional programs. The possible forms of digital image manipulation are literally infinite (Lillesand and Keifer, 1994). Image enhancement is the process of making an image more interpretable to the human eyes. On image the lineaments have been easily identified on the basis of tone, color, texture, pattern and association etc. All possible DIP techniques of edge detection and enhancement have been applied for lineament detection and enhancement.

4.3.1 SPECTRAL ENHANCEMENT

Spectral enhancement deals with the individual values of the pixel in the image. The goal of spectral enhancement is usually to make certain features more visible in an

image by bringing out the contrast. Basically various spatial enhancement techniques like contrast stretching and histogram equalization have been applied to all selected (512×512) windows. The resulting enhanced images help in visual interpretation of joints, fractures, faults and lineaments in the area.

4.3.1.1 Contrast Stretching

In general, it so happens that the number of actually recorded and full dynamic range of the digital image (256 levels) is not utilized. This character is shown in low contrast image of figure 4.1a. Details on such an image are scarcely visible. A simple rescaling of gray levels (linear or non-linear) improve the contrast and details become clearly visible. Figure 4.1b shows the enhanced image after contrast stretching.

4.3.1.2 Histogram Equalization

Histogram equalization is a non-linear stretch which redistribute the pixel values so that there are approximately same number of pixels with each values within a range. The results approximate a flat histogram. Therefore, contrast is increased at the "peaks" of the histogram and lessened at the "tails". Figures 4.2a and 4.2b show the images of unequalized histogram and contrast enhanced image after histogram equalization, respectively.

4.3.2 SPATIAL ENHANCEMENT

Spatial enhancement techniques are characterised by operations over neighborhoods. The brightness value of the image pixels are modified and the new brightness values are derived from the brightness values of a set of surrounding pixels. It is the spatial interdependence of the pixel values that leads to variations in the perceived image geometric details.

4.3.2.1 Convolution Filtering

Spatial enhancement of remote sensing data generally relates to smoothing, edge detection and enhancement and line detection. Enhancement of edges and lines lead to image sharpening. In this method a template, window or kernel is defined and then moved

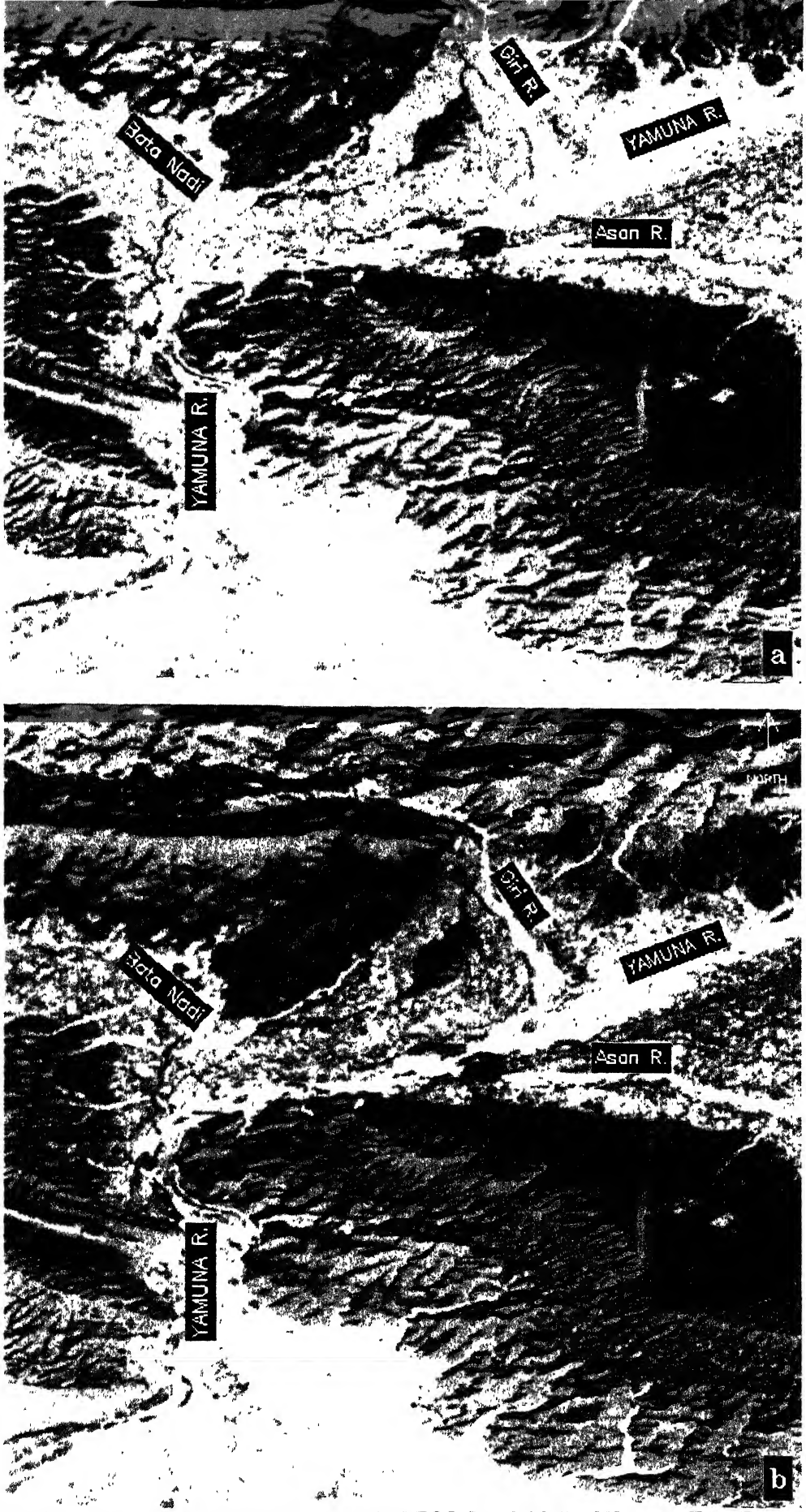

Figure 4.1 a: A typical example of unstreched FCC (band 4,2,1) of Yamuna Tear Fault area
b: FCC (band 4,2,1) of the same area after contrast stretching

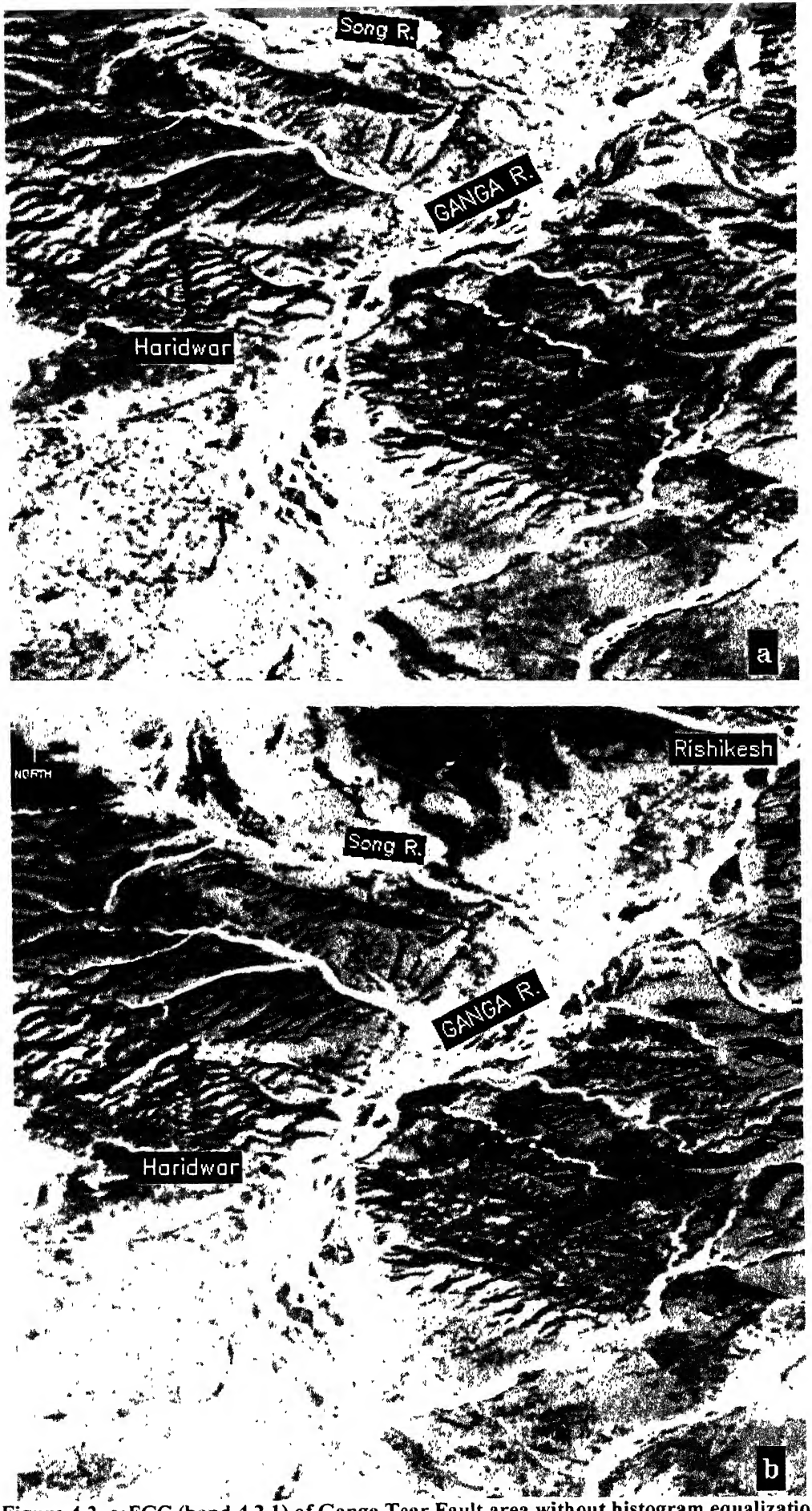

Figure 4.2 a:FCC (band 4,2,1) of Ganga Tear Fault area without histogram equalization
b:FCC (band 4,2,1) of the same area after histogram equalization

over the image row by row or column by column. The products of the pixel brightness values, covered by the template at a particular position and the template entries are taken and summed to give the template response. This response is then used to define a new brightness value for the pixel currently at the center of the template. The following formula has been used to derive an output central image pixel value:

$$V = \text{int}\left[\frac{\sum_{i=1}^{q}\sum_{j=1}^{q} f_{ij} \times d_{ij}}{F}\right] \qquad \text{---------(1)}$$

where,

f_{ij} = the coefficient of a convolution kernel at the position i,j

d_{ij} = image pixel value corresponding to f_{ij}

q = the dimension of the kernel, assuming a square kernel (if q=3, the kernel is 3×3)

F = either the sum of the coefficient of kernel, or 1 if sum of the coefficients of kernel is zero

int = the integer function, which truncate a non - integer number to an integer

V = output pixel value

In case V is less than zero, the value of V is taken as zero. The sum of the coefficients (F) is used as denominator of the equation above, so that the output values will be relatively in the same range as the input values. Since F can not be equal to zero (division by zero is impossible), F is set to 1 if the sum is zero.

4.3.2.2 Edge Detection and Enhancement

Edge enhancement is a simple and effective means for increasing geometric details of an image. In general, edges in remote sensing images are lines of high frequency

variation, which are influenced by terrain properties, vegetation, dislocations of rocks etc. Essentially two methods have been used to detect and enhanced the edges. These are:

(i) by using edge detecting kernel, and

(ii) by subtracting the image resulted by applying the edge detecting kernel from the smoothed image.

The above techniques lead to the enhancement of all high frequency details of an image including edges, lines and points of high gradient. However, the second method gives good results for edge enhancement and lineament delineation. These two approaches are treated in the following steps:

(1) Image Smoothing (Low Pass Filtering):

In this technique, low frequency kernel or low pass kernel has been used to smooth an image. Following low pass filter has been applied on the image to get a smooth image.

$$\begin{vmatrix} 1 & 1 & 1 \\ 1 & 1 & 1 \\ 1 & 1 & 1 \end{vmatrix}$$

Low Pass Filter

Applying the above kernel, equation (1) is reduced to

$$V = \text{int}\left[\frac{\sum_{i=1}^{q}\sum_{j=1}^{q} d_{ij}}{F}\right] \qquad \text{----------(2)}$$

This kernel simply average the value of the pixels, causing them to be more homogeneous (homogeneity is low partial frequency). The resulting image looks

smoother, it retains all low spatial frequency information. All high frequency features, such as edges and lines, are attenuated (Figure 4.3b).

(2) Edge Detection Filtering:

A 3×3 filter has been selected to detect horizontal edges in an image.

$$\begin{vmatrix} 1 & 1 & 1 \\ 0 & 0 & 0 \\ -1 & -1 & -1 \end{vmatrix}$$

Horizontal

The above filter computes a value for the central pixel under the template that is accumulated difference vertically between pixels on three rows spaced two apart. Application of this filter yields the response shown in figure 4.3c. Filters used for detecting edges in vertical and diagonal directions are given as:

$$\begin{vmatrix} 1 & 0 & -1 \\ 1 & 0 & -1 \\ 1 & 0 & -1 \end{vmatrix} \qquad \begin{vmatrix} 1 & 1 & 0 \\ 1 & 0 & -1 \\ 0 & -1 & -1 \end{vmatrix} \qquad \begin{vmatrix} 0 & 1 & 1 \\ -1 & 0 & 1 \\ -1 & -1 & 0 \end{vmatrix}$$

Vertical Diagonal Diagonal

All four 3×3 kernels have been used to the image in order to detect existing edges in all directions. This requires four passes over image data and four separate images have been prepared for each window showing edges in all four directions. As these filters detect only the edges with a background zero value pixels, it is difficult to interpret the resulting filtered images.

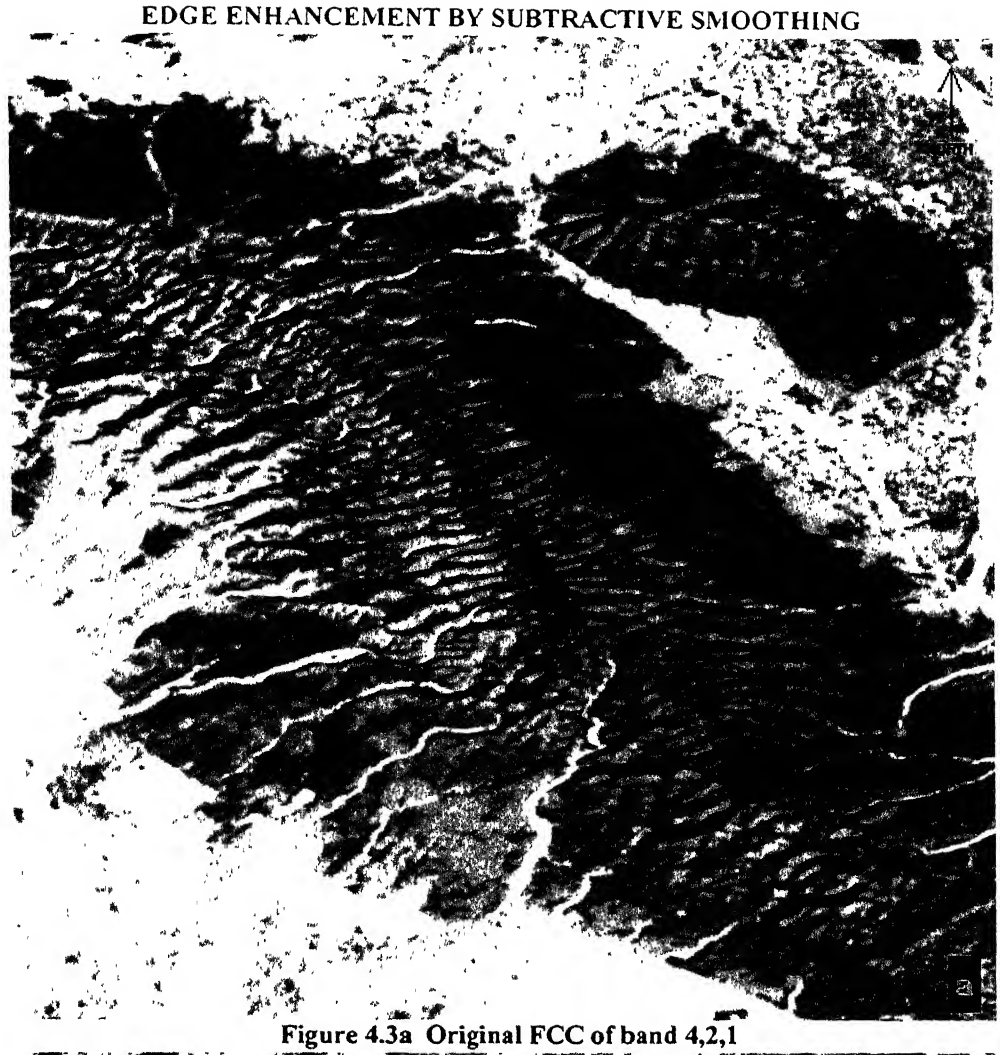

Figure 4.3a Original FCC of band 4,2,1

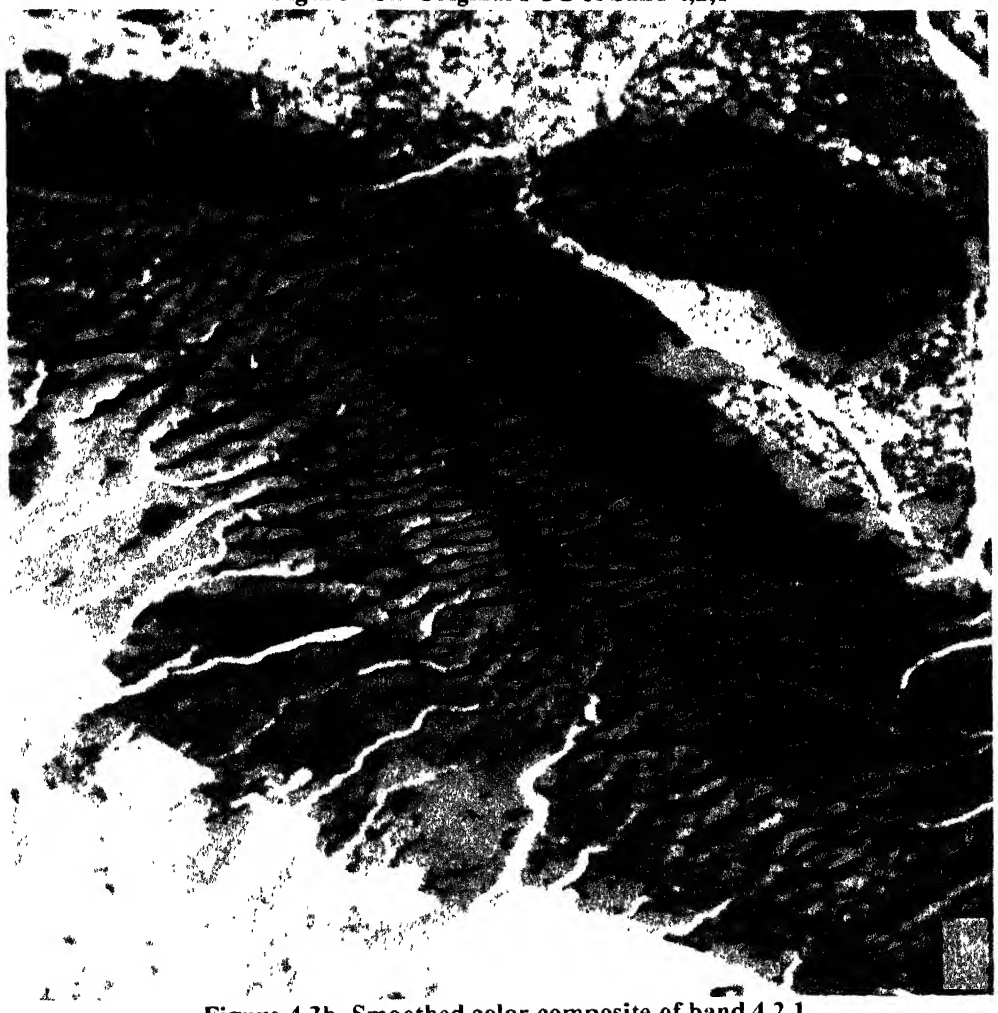

Figure 4.3b Smoothed color composite of band 4,2,1

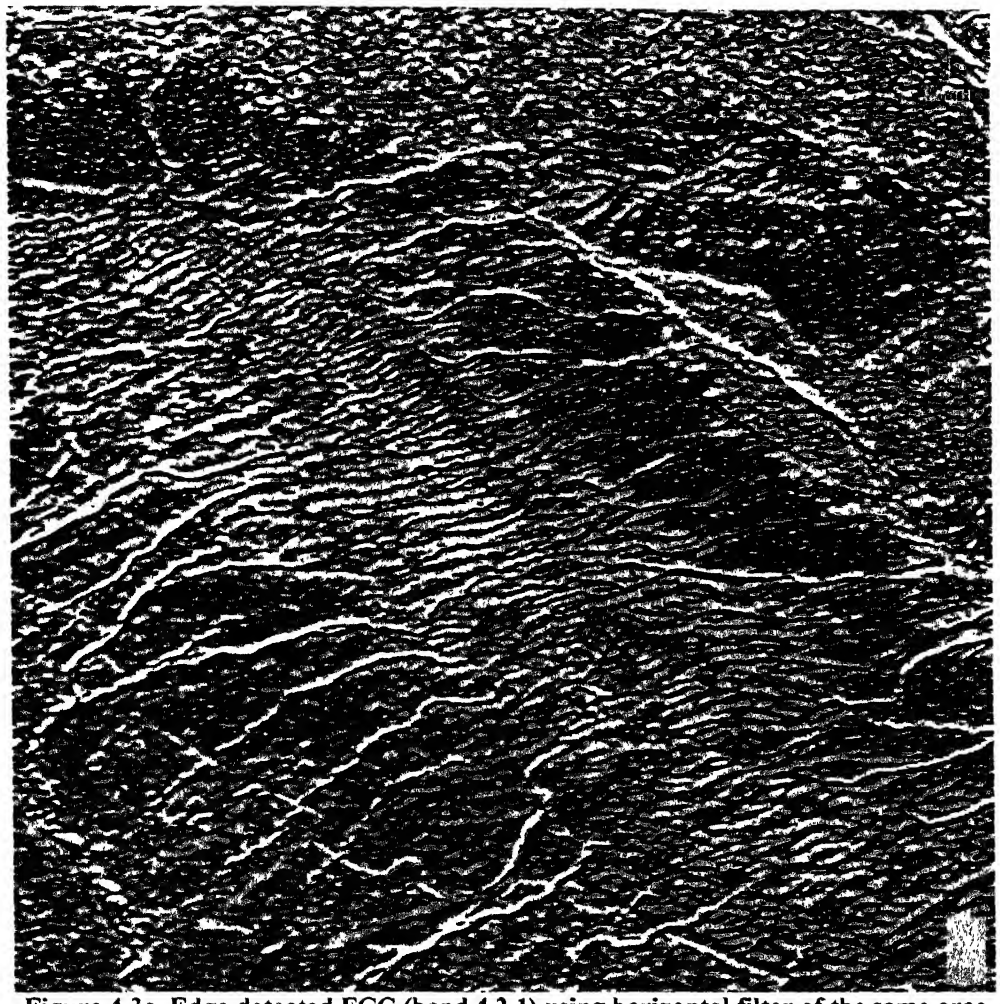

Figure 4.3c Edge detected FCC (band 4,2,1) using horizontal filter of the same area

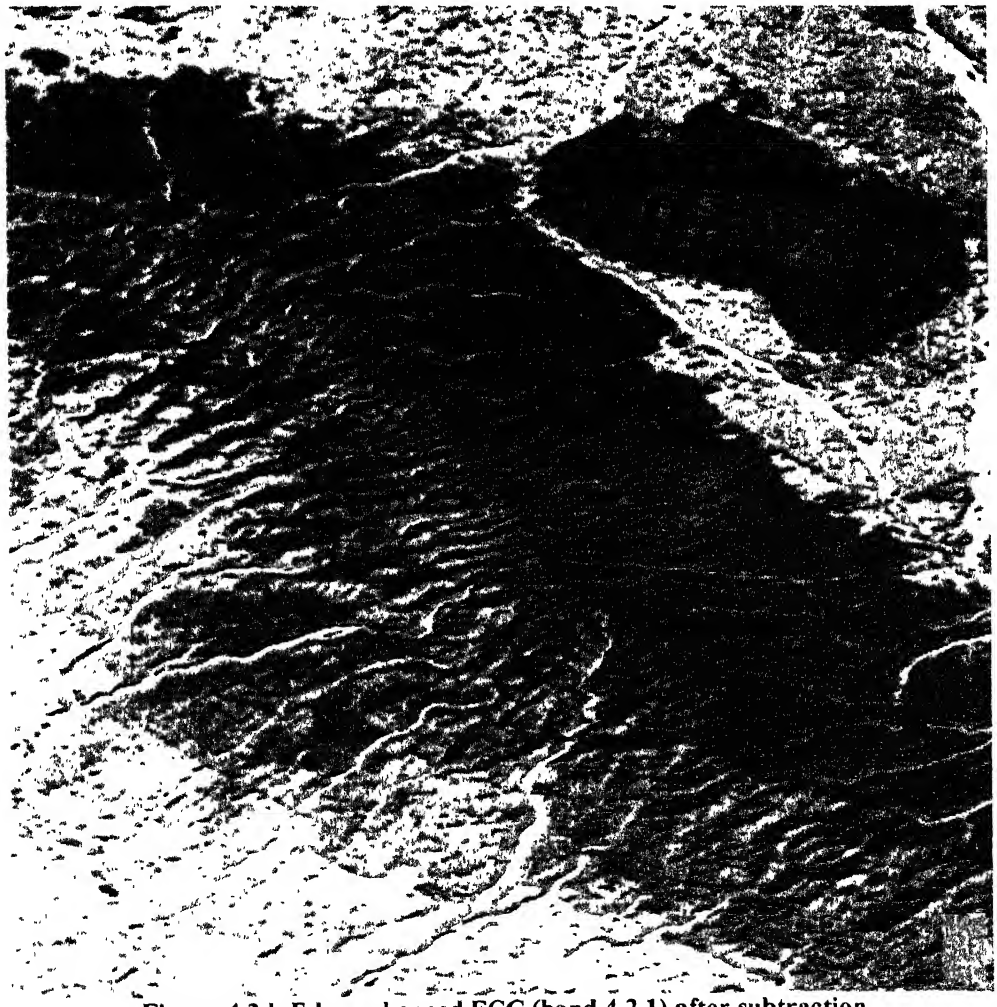

Figure 4.3d Edge enhanced FCC (band 4,2,1) after subtraction

(3) Edge Enhancement by Subtractive Method:

Consequently if the edge detection filtered image is subtracted from the smoothed image, the resultant difference image enhances the edges in a smoothed background. The image after subtraction is shown in figure 4.3d. It is seen that the edges are lines of high reflectance marked by red color in the FCC of band 4,2,1 (Figure 4.3d). Generally, in band 4 (infrared) there is a large variation of pixel values along the dislocations, faults, fractures, stream valleys in hilly terrain. The edge detection filters assigned maximum pixel values along these lines. So they show maximum reflectance after subtracting the edge detected image from the smoothed image of the area in the infrared band.

4.4 LINEAMENT MAPPING

Major faults and lineaments have been mapped by visual interpretation of standard FCC images. Visual interpretation has been carried out based on lithological dislocations, joints and fracture traces, truncation of outcrops, alignment of streams, sudden bending of steams etc. Enhanced edges have been considered to be related to difference in micro-topography, local vegetation, soil type, soil moisture, or micro-fracture, joints, fault scarps, slopes, etc. The edges reflect the micro-lineament patterns of the area. They have been mapped suitably by on-screen digitization of the edges. All possible lineaments have been digitized on the screen from the edge enhanced images in four directions viz. vertical, horizontal and two diagonal directions. Finally, they have been merged with the visually interpreted lineaments in order to get total lineament patterns of the area (Figure 4.4). The artificial linear features like road, canals etc. also got enhanced as edges in DIP techniques. However, these features after comparing from the available information and ground truth have been avoided for the mapping of lineaments. The latitude and longitude of initial and final points of each lineaments have been stored during digitization process for their further statistical treatment.

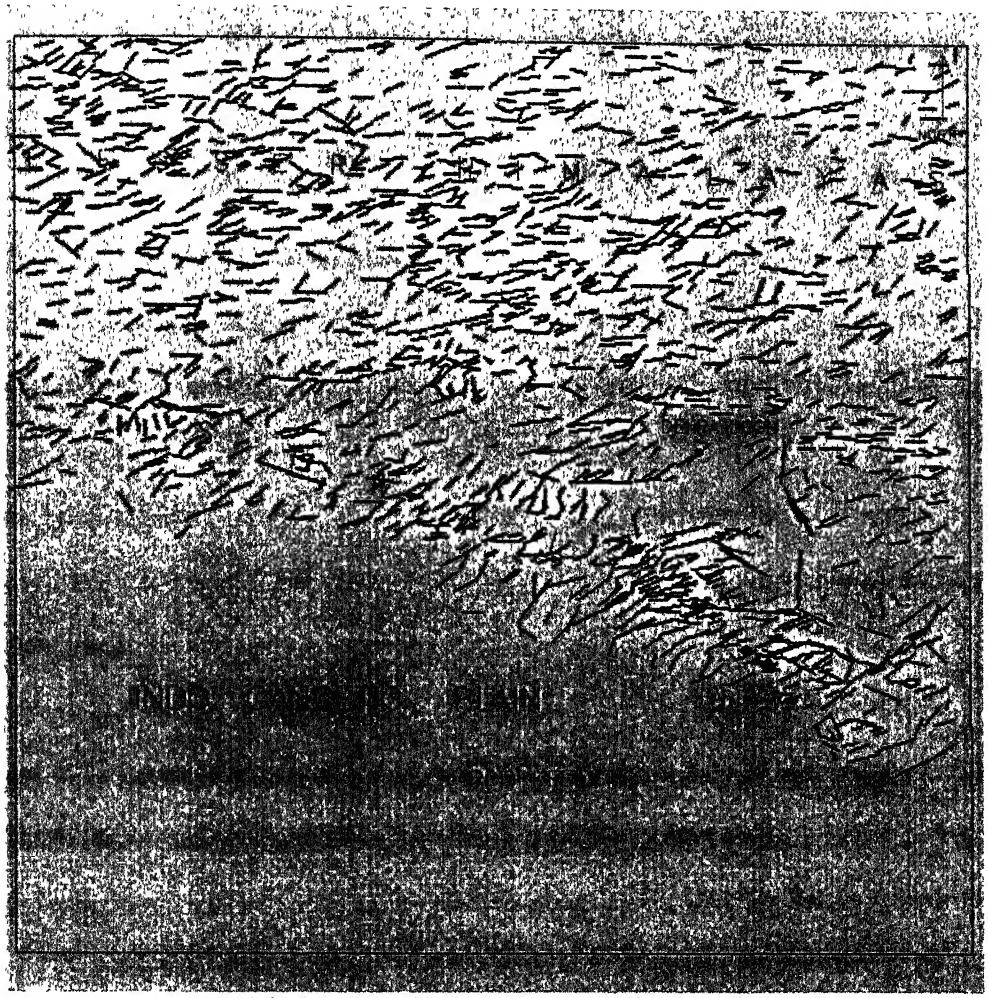

Figure 4.4 Lineament Map of the Area

4.5 STATISTICAL TREATMENT OF LINEAMENT FABRIC DATA

Directional data are an integral part of geological information. Fold axes, faults, joints and many other structural elements show preferably oriented linear patterns on remote sensing data products. These remotely sensed linear features may be measured and treated quantitatively using special statistics that reflect the circular nature of the directional data (Gambel et al., 1953; Mardia, 1972; Gaille and Burt, 1980; Cheeny, 1983).

4.5.1 Basic Concept of Rose Diagram

Rose diagram is circular histogram used by most Geologists to portray distribution of directional data. It is a plot of class frequency on a compass rose. Directions of the lineaments have been plotted in a compass rose, relative abundance of the data in that direction (Dennison, 1968). The procedure violets one concept of histogram theory, the area plotted for class is not proportional to class abundance. The area of the segment of a circle is given by:

Area = $C/360 * \pi r^2$

where, C is equal degrees arc of segment and r is the radius of arc segment. But radius is proportional to square root of number of individuals in that class.

4.5.2 Rose Diagram of Lineament Fabric Data by Computer Programming

A computer program has been written in C language (Appendix I) to plot the rose diagram of the remotely sensed lineament fabric. The program has been designed in three parts for three different applications. The first part deals with the rose diagram plotting, second part estimates the stress direction from the lineament orientations and third part extract the active faults and lineaments from remotely sensed lineament fabric data which have been described in sections 4.6 and 4.7, respectively.

The algorithm to plot the rose diagram is based on the basic concept of rose diagram. The latitude and longitude values of initial and final points of each lineament

have been taken as input from the ERDAS digitize file and the slope of the lines has been calculated using the following formula:

$$slope = \frac{(\ln_f - \ln_i)}{(\mathrm{lt}_f - \mathrm{lt}_i)} \qquad \text{----------(3)}$$

where, $\ln_i$, and lt_i are the longitude and latitude of initial point of the lineament respectively and $\ln_f$, and lt_f are the longitude and latitude value of the final point of the lineament, respectively.

The slope of each lineament has been calculated by the above procedure and grouped into classes for a particular class interval (α) from the north. Data has been generated making compatible to GRAPHER software package to plot the rose diagram of the lineament data. Here the radius of rose diagram for particular class is equal to the square root of number of lineaments in that class. Figure 4.5 shows image of a 512×512 window with lineaments and corresponding rose diagram. Similar procedures have been followed for all selected windows. and rose diagrams have been plotted. Finally, the rose diagrams of all windows are mosaic in one plane fixing the center of each rose diagram in the central longitude and latitude of their corresponding windows (Figure 4.6).

Rose diagram (Figure 4.6) of lineament fabric reveals drastic change of lineament pattern in the north and south of MBT. In the Lesser Himalayan region, maximum number of lineaments oriented in east-west direction (N 80^0-90^0 E). In Dun valley and Siwalik region the trend of majority of lineaments is found to be N 40^0-50^0 E.

4.6 TECTONIC STRESS ESTIMATION FROM REMOTELY SENSED LINEAMENT DATA

There is a strong evidence from laboratory and field observations that the orientation of fault planes are primarily controlled by the direction of principal stress.

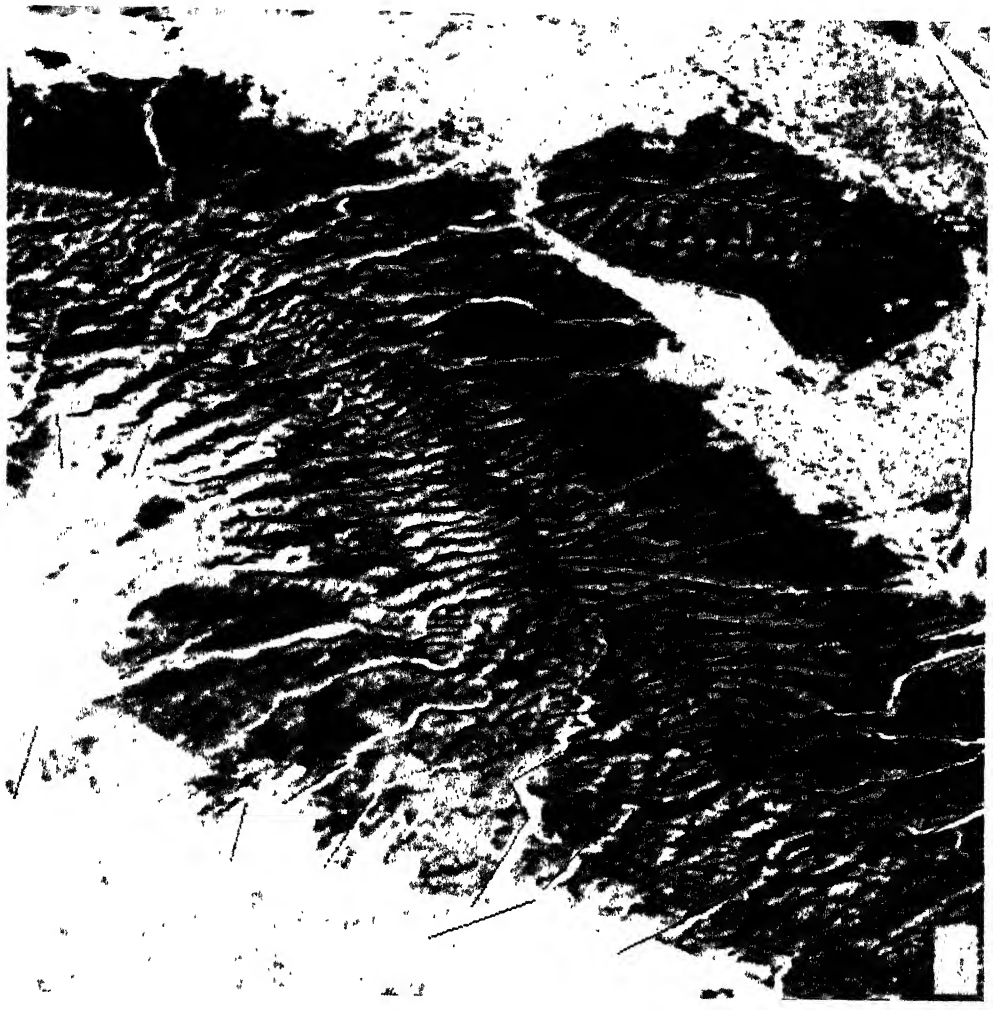

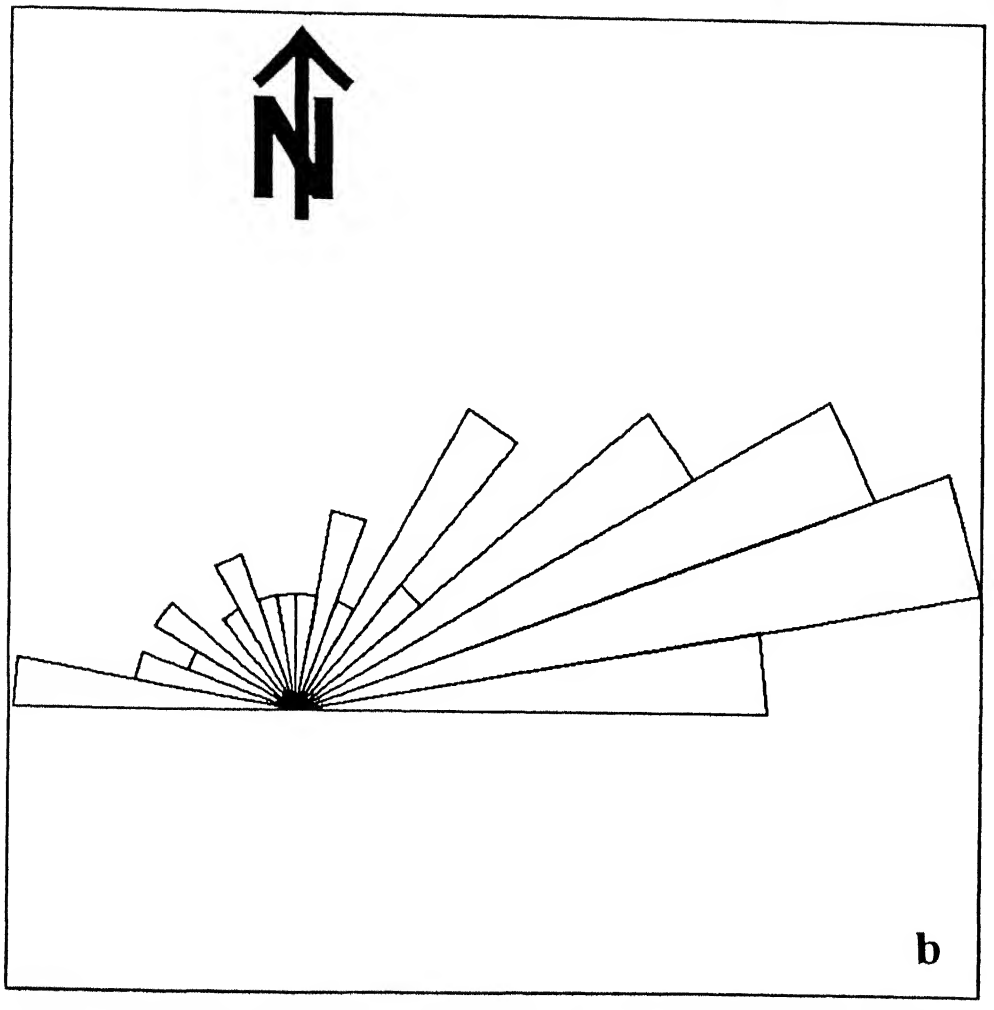

Figure 4.5 a: FCC (band 4,2,1) image overlapped with lineaments; b: Rose diagram showing orientation of lineaments (shown in figure 4.6a) from north at 10^0 intervals.

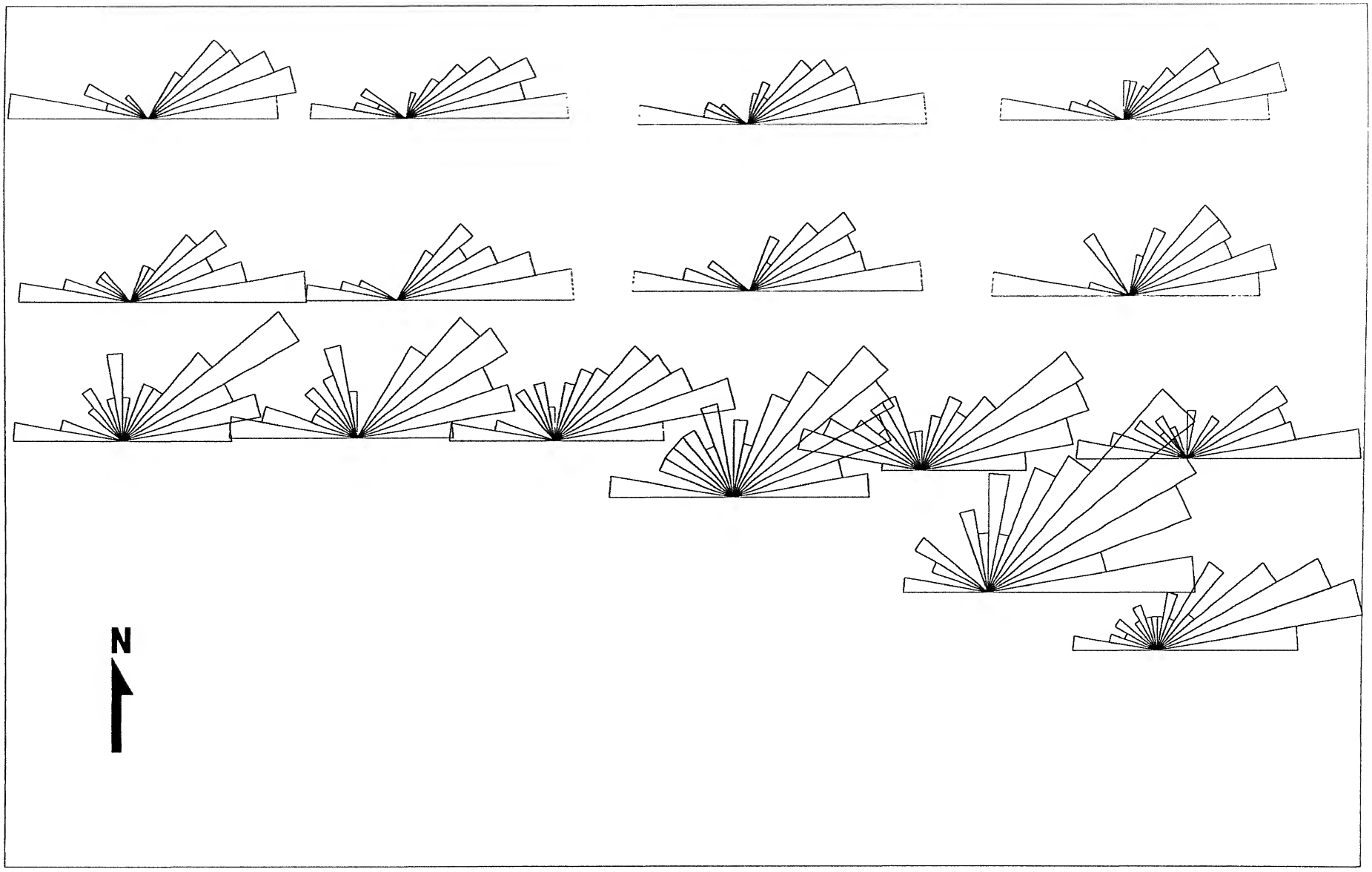

Figure 4.6 Rose diagram showing orientation of lineaments from north at 10° intervals at various locations in the area

Thus, the principal stress direction (σ_1) can be determined from the orientation of fault plane. Quantification of fault plane orientation with respect to principal stress direction is of paramount importance in structural analysis. The work performed by tectonic forces on the fault zones are completely consumed within this zone (Mandle, 1988). This imposes an important restriction on the sense of displacement along a fault. The mechanical work done per square cm of its surface, by definition, is the product of shear stress (S) on the fault plane and the relative displacement of the fault blocks. The shear stress in this product is the component parallel to the line of the relative displacement. Since the mechanical work is supplied to the fault zone proper, the product is considered to be positive; otherwise, mechanical work would be extracted from the fault. Both shear stress and fault plane must therefore have same sign and hence point in the same direction of the maximum compressive stress (i.e. the maximum principal stress σ_1) has to make an acute angle (θ) with direction of the fault displacement. For determination of angle "θ" more accurately, Mohr's theory of failure for granular material is taken into consideration which is briefly discussed in the next section.

4.6.1 MOHR'S THEORY OF FAILURE

German engineer Otto Mohr put forwarded the theory of failure in the year 1882. According to which the shear stress in the plane reaches at the peak, an apex value that depends upon the normal stress acting in that plane and the property of the material constituting the failure surface. This represents that the orientation of discrete slip elements, along which the material deforms in the limit state, is determined oy the interaction of shearing and the normal stress. Based on Mohr's theory, the shear strength of a given rock is a function of the normal stress and the mineral properties (e.g. strength parameters, cohesion 'c' and internal angle of friction "ϕ"). Thus, shear strength of a material having cohesion 'c' can be represented by

$$S = c + \sigma \tan \phi \qquad \text{------(1)}$$

where S = shear strength of the material and σ = normal stress at the failure surface.

The plot of s-σ relation over the Mohr's diagram is shown in figure 4.7. Some basic relationships deduced from Mohr's circle are (Cernica, 1995):

(i) The maximum shear stress is equal to the radius of the circle. Furthermore, the maximum shear stress is on a plane that makes an angle 45° at any point on the Mohr's circle makes an angle 2θ (θ is angle between the failure plane and σ_1 direction).

(ii) The line satisfying equation (4) is drawn tangential to the Mohr's circle. It is described as Mohr's envelope. Note that the shear stress in this plane is less than S_{max}. Interestingly, one can note that slip occurs at the point of maximum obliquity and not at the angle where S_{max} occur. It is therefore the angle of obliquity (ϕ) that assumes the position of slip.

(iii) Any combination of stress that falls within the envelope represents a stable condition. The tangent to the Mohr's circle, thereby, depicts a condition of impending failure. The corresponding points of tangency represent the resultant to shear and normal stresses in the failure plane.

From figure 4.7, the orientation of the failure plane with reference to the plane of major principal stress in a granular material may be readily established as

$$2\theta_{cr} = 90+\phi$$

$$\theta_{cr} = 90/2 + \phi/2 = 45 + \phi/2$$

$$\theta = 90 - \theta_{cr} = 45 - \phi/2$$

$$\theta = 45 - \phi/2 \qquad \text{-------(5)}$$

where, θ_{cr} is critical angle of failure plane with the σ_3 direction and θ is angle between failure plane and σ_1 direction.

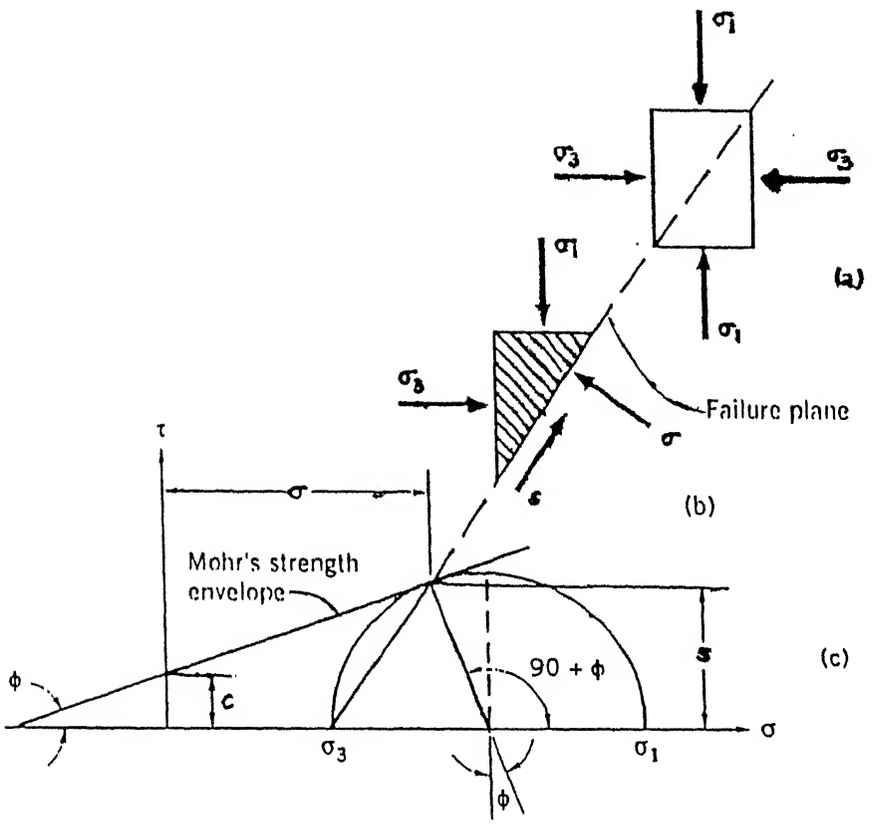

Figure 4.7 Mohr's circle of stress condition. (a) Element, $\sigma_1 \geq \sigma_3$; (b) Normal and shear stress on the plane of failure; (c) Mohr's circle of stress condition shown in (a) (after Cernica, 1995)

In the present context, most of the lineaments and faults represent slip faces, which have been considered as the result of continued horizontal maximum compressive stress ($S_{H\max}$) due to Indian plate movement against Eurasian plate. The direction of stress acted on each element of failure has been estimated using equation (5).

Part II of the computer programme deals with the estimation of stress direction from the lineament pattern using standard ϕ value of the rocks present in the study area (Appendix II). The ϕ values of 25^0, 30^0 and 33^0 have been considered for Dun gravels, Siwalik sandstone and Lesser Himalayan metamorphics, respectively. The orientation of stress acting on each lineament with respect to north has been calculated and grouped into classes of 10° interval. This procedure has been repeated in each selected windows of 512 ×512 pixel dimension and the results have been plotted as rose diagrams. Finally, each rose diagram is assigned to its appropriate position in the main scene with respect to their positions in terms of longitude and latitude (Figure 4.8). The stress map of the area has been prepared taking the angle of maximum frequency of stress rose diagram as $S_{H\max}$ orientation (Figure 4.9). The $S_{H\max}$ orientation at different sites determined by above method is also given in table 4.2.

Above data shows that average $S_{H\max}$ direction of all sites of Lesser Himalayan range is N 50^0-60^0 E. In Dun valley and Siwalik range average $S_{H\max}$ orientation is N 20^0-30^0 E, except the Yamuna tear fault (site no. 16) and Dhaulakhand fault (site no. 18) area, the orientation is found to be in the range N 40^0-50^0 E. Lesser Himalayan rocks are older than Siwaliks and has undergone earlier phase of deformation. From the data it can be interpreted that during Lesser Himalayan phase of deformation, the maximum horizontal compressive stress ($S_{H\max}$) was in N 50^0-60^0 E and gradually it has rotated counter clock wise about 30^0 to N 20^0-30^0 E till end of Siwalik phase of deformation (Pleistocene age). This interpretation can be correlated to anti clockwise rotation of Indian plate after collision with the Eurasian plate (Molnar and Tapponnier, 1978)

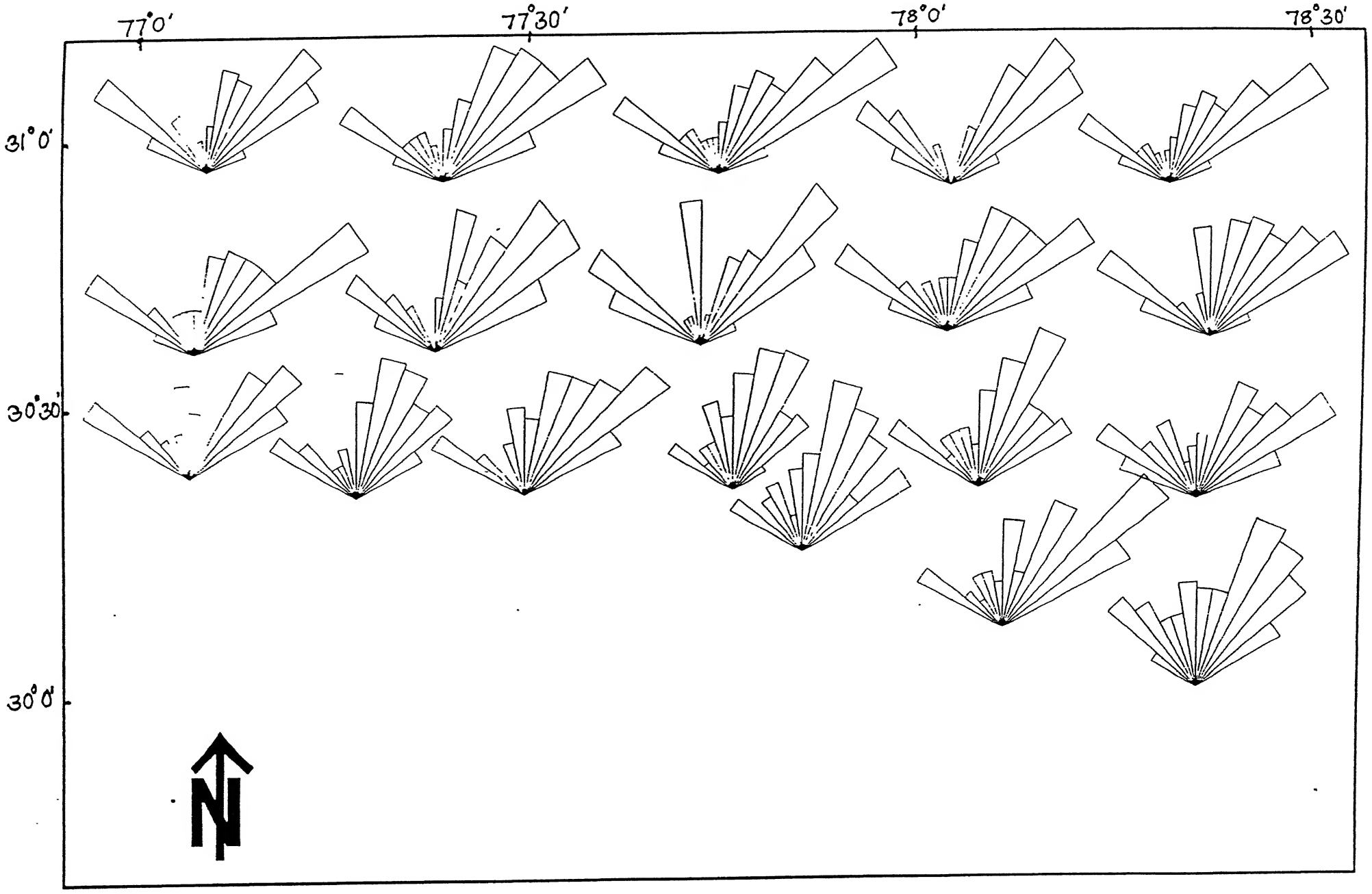

Figure 4.8 Rose diagram showing orientation of maximum horizontal compressive stress from north at 10° intervals at different sites in the area

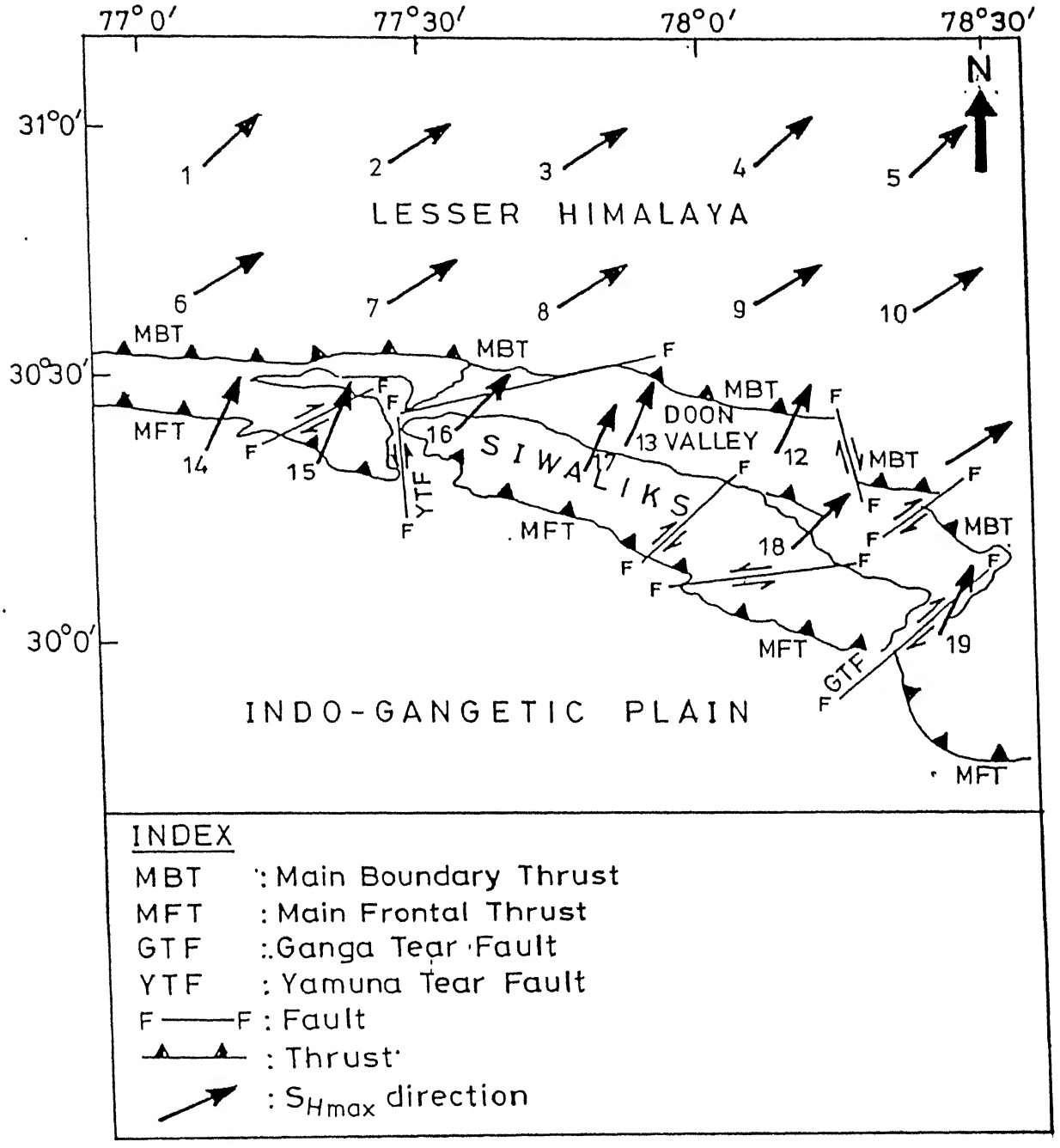

Figure 4.9 Stress map of the area showing S_{Hmax} direction

Table 4.2 S_{Hmax} orientation at different sites derived from remotely sensed lineament data.

Site No.	Longitude	Latitude	Azimuth (^{0} from N)	Region
1	77.08	30.95	40 - 50	Lesser
2	77.41	30.95	50 - 60	Himalaya
3	77.74	30.95	50 - 60	
4	78.07	30.95	40 -50	
5	78.36	30.95	40 - 50	
6	77.08	30.68	50 - 60	
7	77.41	30.68	50 - 60	
8	77.74	30.68	50 - 60	
9	78.07	30.68	50 - 60	
10	78.36	30.68	50 - 60	
11	78.34	30.35	50 - 60	
12	78.34	30.42	20 - 30	Dun Valley
13	77.78	30.37	20 - 30	
14	77.08	30.42	20 - 30	Siwaliks
15	77.27	30.42	20 - 30	
16	77.53	30.42	40 - 50	
17	77.78	30.42	20 - 30	
18	78.08	30.17	40 - 50	
19	78.34	30.02	20 - 30	

4.7 DELINEATION OF ACTIVE FAULTS AND LINEAMENTS FROM LINEAMENT FABRIC DATA

Using three different stress indicators i.e. borehole elongation breakouts, in-situ hydrofracturing measurement and earthquake focal mechanism, Gowd et al. (1992) have prepared the maximum horizontal stress (S_{Hmax}) orientation regime of the Indian sub-continent which is incorporated in the world stress map. Extracting the stress direction data of the study area (Table 4.2) from the stress map of India (Gowd et al., 1992), it is extrapolated that maximum horizontal compressive stress acting in this region is N 23^0 E.

Computer program (part III) has been developed to delineate those lineaments of figure 4.4, which are showing maximum stress direction within the range varying from N 20^0 E to N 30^0 E. A fair assumption, that the active stress direction is taken at an interval of 10^0 instead of a particular value, is authentic as the study area comprises of different rock types of varying ϕ values and other inhomogeneity.

Table 4.3 S_{Hmax} Orientations in North West Himalaya Derived from Focal Mechanism of Earthquakes

Latitude (^{0} N)	Longitude (^{0} E)	Magnitude	Azimuth
31.92	78.61	5.1	23
30.75	78.75	-	42
29.93	80.27	5.7	190
30.1	80.7	6.2	207
29.7	80.9	6.1	212
29.7	80.9	5.8	190
29.63	81.09	6.1	195
29.34	81.21	5.7	180

(after Gowd et al., 1992)

The algorithm used by this computer program is based on equation (5). It determines the orientation of all lineaments with respect to north and their respective maximum stress direction. Then it compares the resulting maximum stress direction with the stress due to Indian plate motion (N 20^0-30^0 E). The lineaments developed due to stress (N 20^0-30^0 E) by the Indian plate motion have been extracted from the whole lineament fabric data and written in digitized ERDAS file format to display only the active lineaments. The active lineament map thus, prepared is shown in figure 4.10.

From the map it is seen that the number of active lineaments in the Siwalik and the Dun valley are more as compared to Lesser Himalayan range and the concentration of active lineaments is maximum in the intervening zone between Ganga and Yamuna tear faults. This indicates the tectonically active nature of the area lying south of MBT.

4.8 MULTI-DATA INTEGRATION AND INTERPRETATION (GIS APPROACH)

4.8.1 Geographic Information System (GIS)

The importance of Geographic Information System (GIS) has been realized in integrated geo-investigation studies. The purpose of GIS is to turn the geographic data into information - the answer to the real life questions. For simplicity, it can be defined as "automated tools for the efficient storage, analysis and presentation of geographic data." (Gupta, 1991). The GIS aims at storage and retrieval of all types of data at particular geographic location. Broadly, it includes all possible types of information - geological (rock types, structure etc.), geophysical (magnetic, electric, gravity etc.), remote sensing, topographical (slope, elevation etc.), and all other possible types of data. The data are superimposed using a common reference geographic grid. Any set of data relevant to a particular investigation for a particular area can be retrieved from GIS.

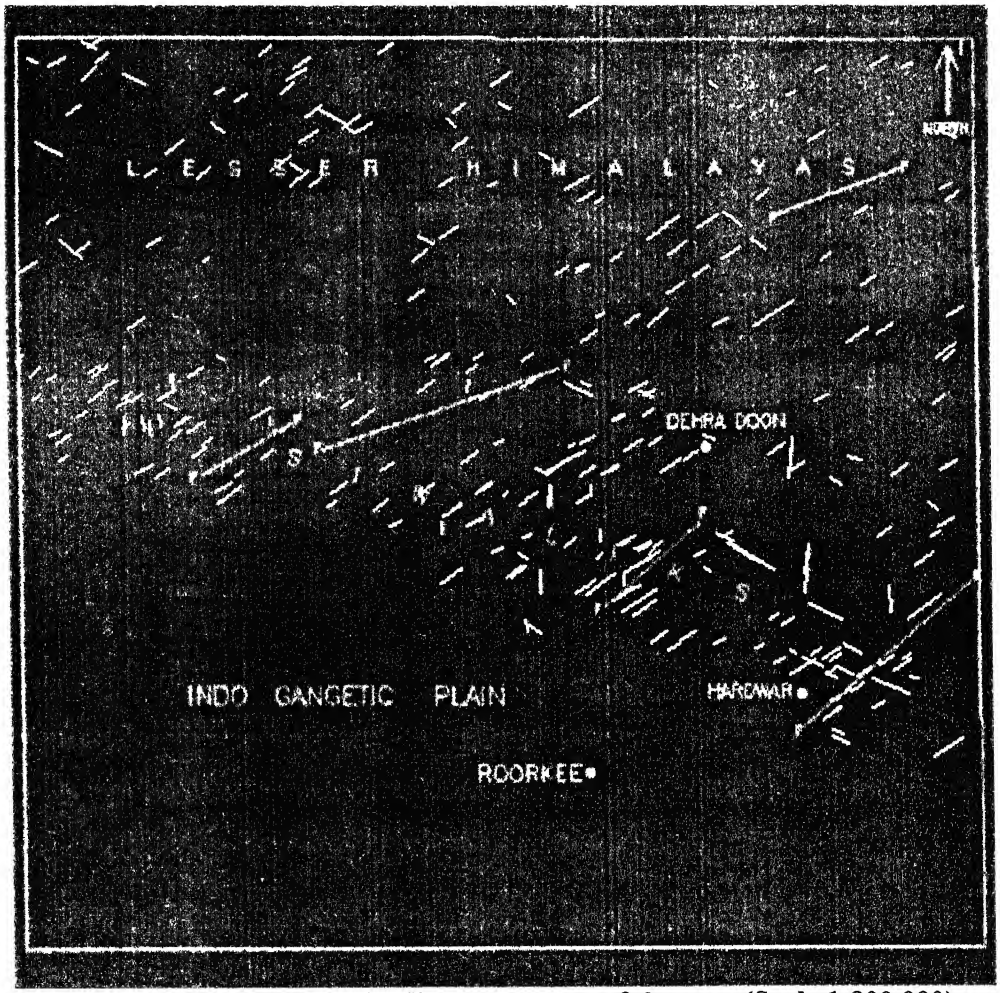

Figure 4.10 Recently active lineament map of the area (Scale 1:800 000)

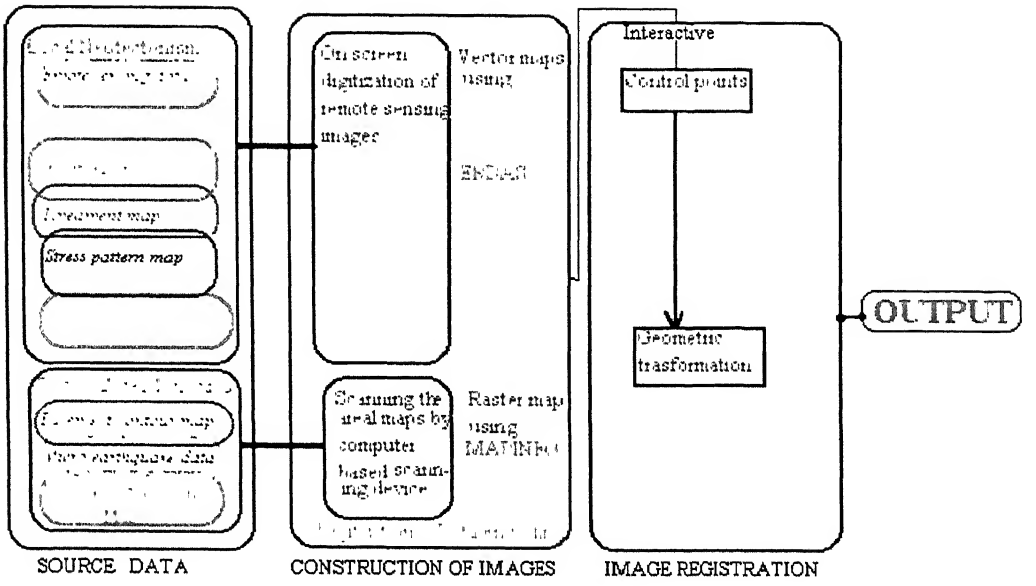

Figure 4.11 Steps carried out to generate multi-geodata sets i.e. GIS

Various data sets reconstructed from remote sensing spectral data, in the form of lithological, structural, lineament maps, etc. are of obvious important for obtaining a GIS based local neotectonic map of the area. Similarly, the depth to basement contour map, historical earthquake data (Figure 2.4) and the A, b value relative seismicity map (Figure 2.3), are helpful in developing a regional scale geodynamic model. The latter when assessed in terms of the local neotectonic maps of the study area, provides some factual clues to solve many Himalayan mysteries. The steps carried out to reconstruct the GIS for the above described purposes are shown in the figure 4.11.

4.8.2 Neotectonic Study of the Area Using GIS

Lithological, structural, lineament, stress and active lineament maps have been considered to be relevant for the neotectonic interpretation of the area. All such maps have been prepared by on screen digitization over remote sensing images in the vector format using ERDAS package. All the acquired images are from the same ground element. Therefore, all the images have been registered or superimposed easily by raster GIS modules of ERDAS. The different thematic maps showing neotectonism of the area are shown in figures 4.12 and 4.13.

Besides MBT and MFT other tectonic features in the area are shown in the figure 4.12. Among them Ganga Tear Fault (GTF), Dhaulakhand fault and Yamuna Tear Fault (YTF) are major strike-slip faults running transverse to the Siwalik range. Both MBT and MFT are found to be disrupted by YTF and GTF which indicate the transverse strike-slip faults which are the youngest tectonic features of the area. The displacement directions of different blocks in the region reveal that the whole region between YTF and GTF have moved relatively more in north-east direction.

4.8.3 PRESENT DAY GEODYNAMIC FRAMEWORK OF THE REGION USING GIS

The tectonic features of the study area is believed to be related to the collision of Indian plate against the Eurasian plate. However, the remote sensing data of small area is

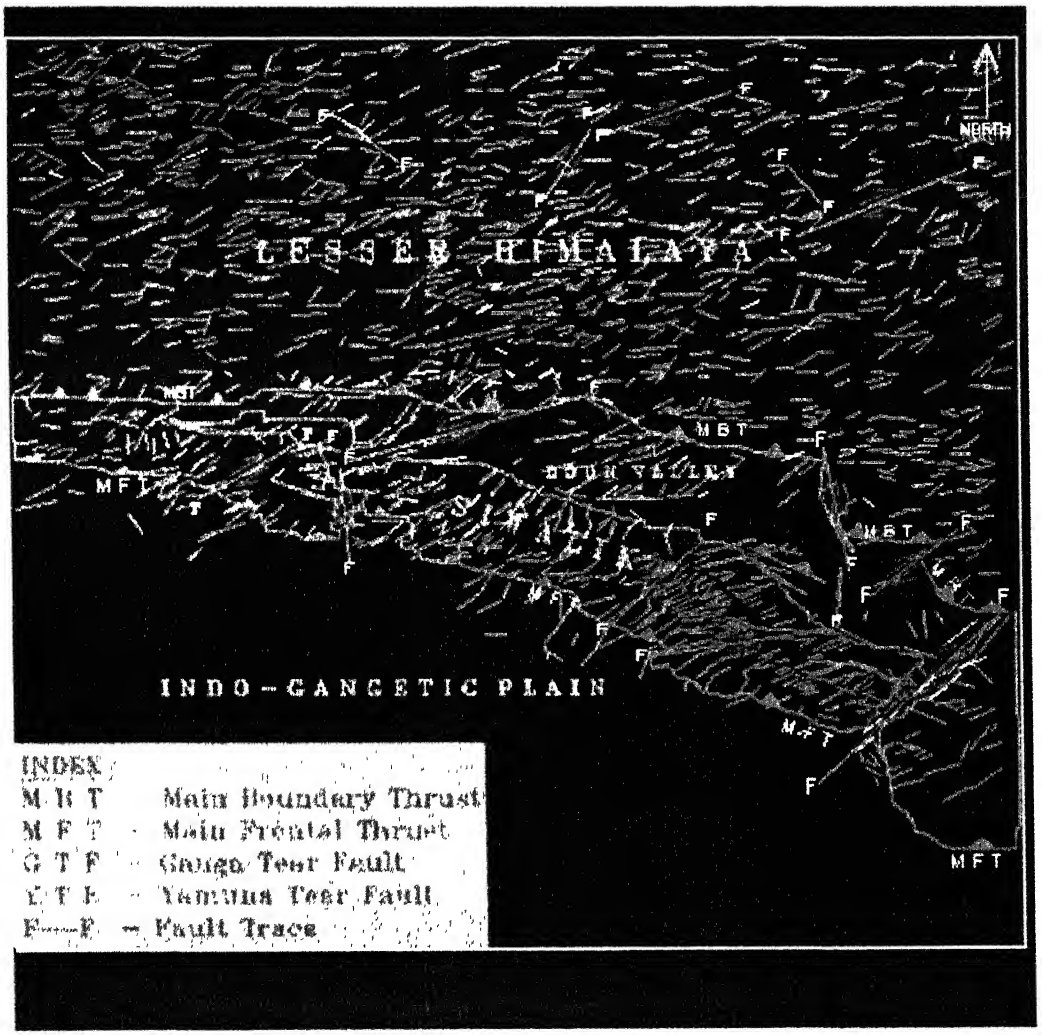

Figure 4.12 Tectonic - Lineament Map of the Area (Scale 1: 800 000)

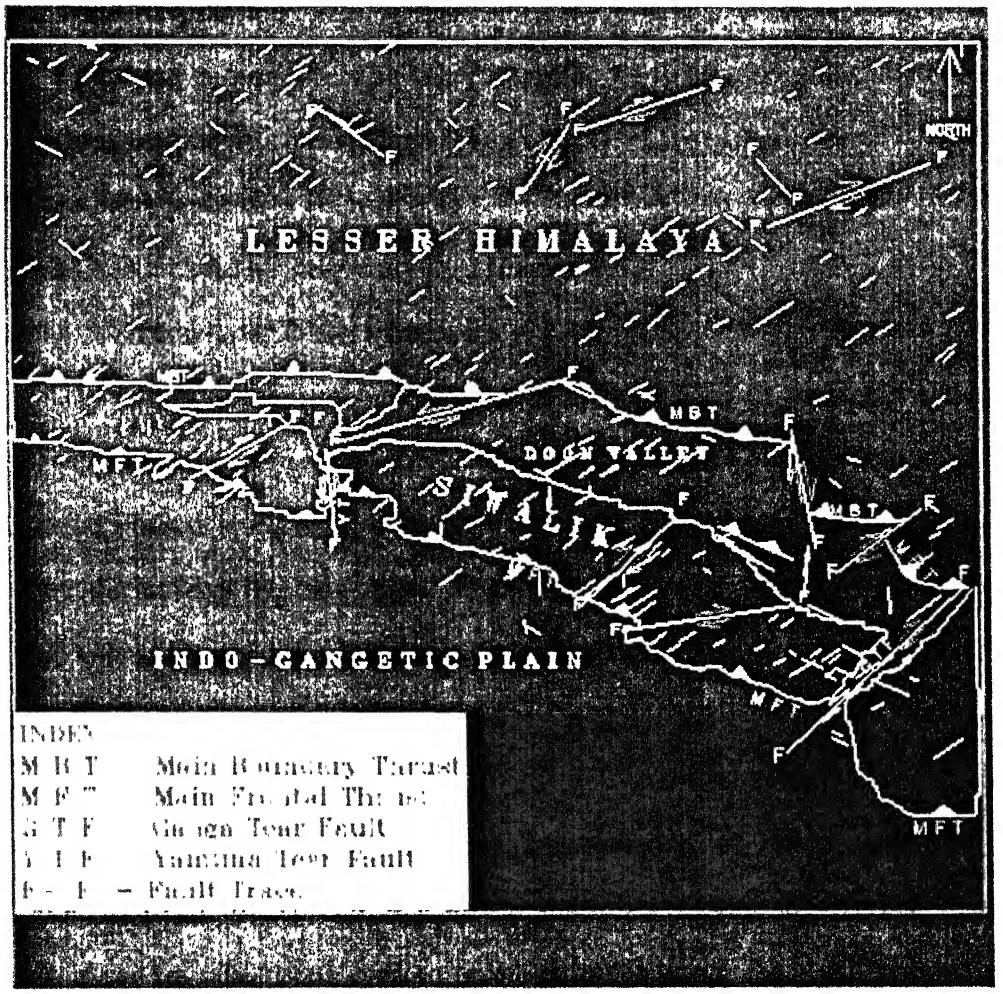

Figure 4.13 Tectonic - Active lineament Map of the Area (Scale 1 : 800 000)

not found sufficient to correlate with the existing tectonic features of the area in the regional geodynamic framework operating in the region. Therefore, a wide area (latitude 28^0 - 32^0 N, longitude 74^0 - 82^0 E) has been selected for developing a regional geodynamic model and to interpret the tectonic elements of the study area.

4.8.3.1 Data Acquisition

Following geo-data sets have been considered to be relevant for the above study.

(1) The basement depth contour map (Figure 4.14)

(2) Micro-earthquake data (Figure 2.4)

(3) A and b value relative seismicity map (Figure 2.3)

4.8.3.2 Construction of Digital Imagery

The multi-geodata sets have been derived from different sources are in the form of aerial maps showing different attributes. Digital images have been generated with the help of computer based scanning system and have been incorporated into the computer. The scanning device digitizes the maps directly and encoded them in vector format. The scanned vector images have been converted into raster images using MAPINFO (Figure 4.11).

4.8.3.3 Image Registration

The next step before integrated interpretation of image data sets has been attempted to geometrically superimpose the multi-data sets i.e. registration. The images or original maps have been analysed to locate prominent and easily defined points such as important cities, prominent topographical features etc. Minimum three points in each image are required to fix the coordinate of the whole image. These are used as control points for registration. Using the identified control points, the image data are registered over one another with the help of MAPINFO GIS software. Various collateral data from different sources have been superimposed and a GIS has been designed to generate a regional plate tectonic model of the area.

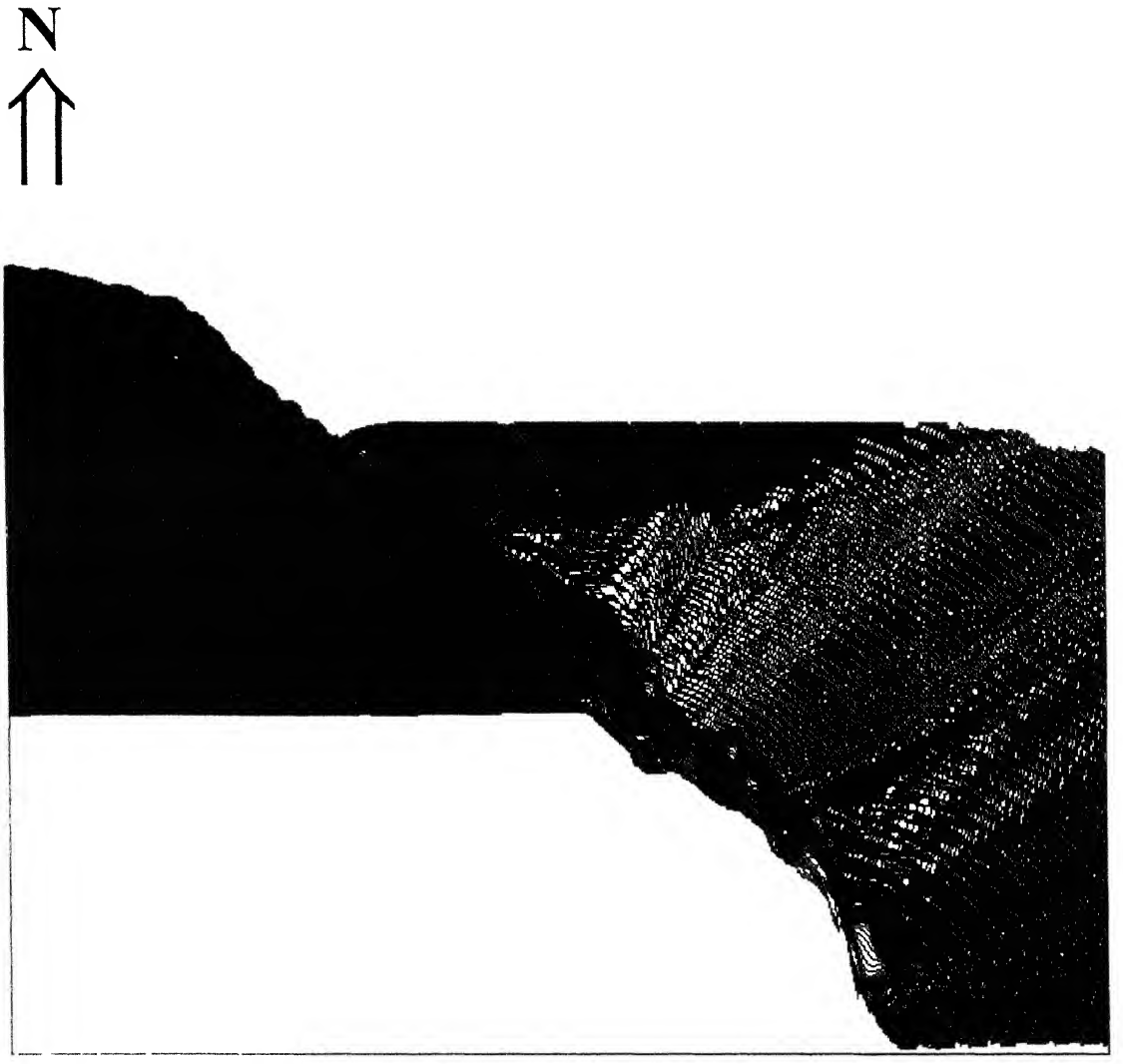

Figure 4.15 Digital Elevation Model generated by IDRISI showing basement topography

4.8.3.4 DIGITAL ELEVATION MODEL OF BASEMENT

The Digital Elevation Model (DEM) of basement in the selected region has been generated using IDRISI. It provides an idea about the basement topography of subducting Indian plate. However, there is a very poor availability of basement topography data over whole region. So the basement contours for the whole region has been interpolated from the available contours and DEM has been generated (Figure 4.14). From the DEM, it is clear that the basement topography of Indian plate is uneven in the region. The basement highs in the south western part represent the Aravalli-Delhi surface massif/uplift. The striking feature of the region is the DHR. It is an elongated basement ridge, lying between (longitude 76^0-79^0 E, latitude 28^0-30^0 N), starts from Delhi and extends towards north in north-east direction through Hardwar. DHR has been considered as the northward extension of Delhi-Aravalli massif. Overlapping the geographical location map over it reveals that the DHR is lying between Ganga and Yamuna rivers. The trend of DHR is about N 23^0 E which coincides with the stress direction estimated from lineament fabric data.

4.9 REGIONAL GEODYNAMIC FRAMEWORK AND ORIGIN OF GTF AND YTF

DEM of basement shows that the Peninsular rocks continue to extends below Siwalik range and one such subsurface feature is DHR. A regional geodynamic model has been put forward considering the regional and local tectonic features of the area (Figure 4.17). The compression that was responsible for Indian-Asian plate collision and consequent formation of Himalayan orogen, though subdued, has not yet ceased. A large number of earthquakes occurring between MBT and MFT bear testimony to the continued compressional stress regime (Routela and Sati, 1996).

The uplift of Siwalik between MBT and MFT has caused its tilting towards north-west and development of many intra-basinal faults (Valdiya, 1986). The tectonic features of Siwalik are consistent with stress imposed by Indian plate movement. The lithospheric

THEMATIC MAP GENERATED BY MAPINFO

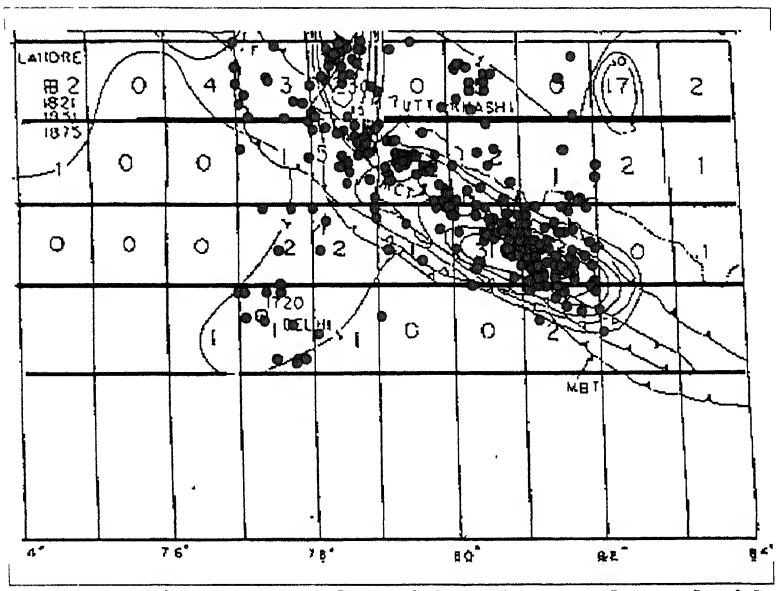

Figure 4.16a Relative Seismicity Map overlapped with earthquake data (magnitude ≥ 4.0 for the period 1720-1995)

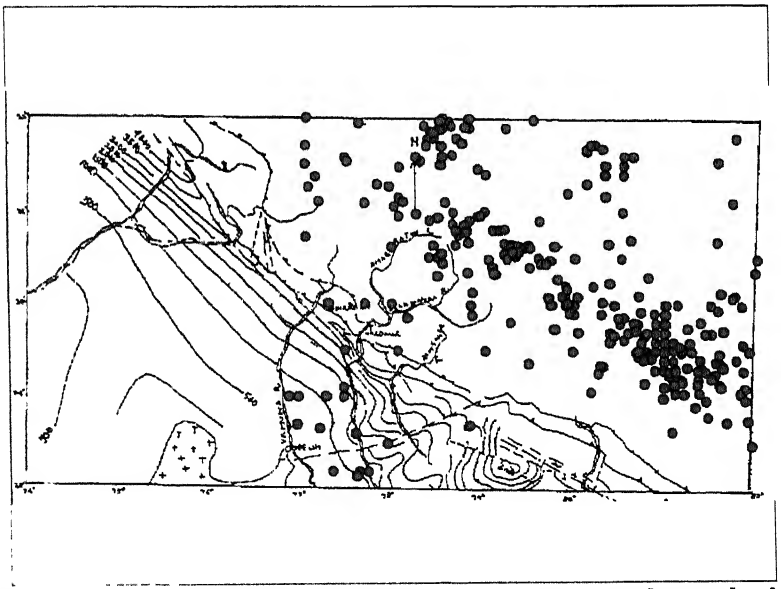

Figure 4.16b Basement depth contour map overlapped with earthquake data (magnitude ≥ 4.0 for the period 1720-1995)

basement high (DHR) seems to be responsible for the development of transverse strike-slip faults in Siwalik and Lesser Himalayas. According to Raval (1995), the non-uniformity of under thrusting Indian plate in the form of basement ridges would act as barrier within the thrust which in turn would control the stress distribution along the collision axis. The dip angle at which Indian slab is subducting beneath Tibet is also affected by basement ridges such that part containing basement ridge will bend at a shallower angle compared to those which do not have basement ridge. As the Indian plate with DHR is subducting below the Himalayan rock piles, the whole zone along with Siwalik above DHR is uplifting and moving in NE direction. The rising of intervening region between Ganga and Yamuna rivers has also been reported by geodetic measurement and geologic study by several workers (Gahalaut and Chandra, 1992; Philip, 1996). The rising and unequal horizontal displacement of Siwalik in north-east direction due to DHR cause the development of sinistral YTF and dextral GTF. Both the Ganga and Yamuna river flowing parallel and migrating away from each other are structurally controlled by DHR.

Superimposition of earthquake data of last two hundred years indicate the seismically active nature of DHR region (Figure 4.16). The stress due to plate motion is effectively transmitted to large distance and get localized at the basement ridges (Raval, 1991). The concentration of stress along the transverse DHR activate the existing transverse faults and lineaments and resulting larger earthquakes in the region. The active lineaments delineated from the remotely sensed lineament fabric shows maximum number of active faults in the region between Ganga and Yamuna river, which can be correlated with the seismically active Delhi-Hardwar ridge.

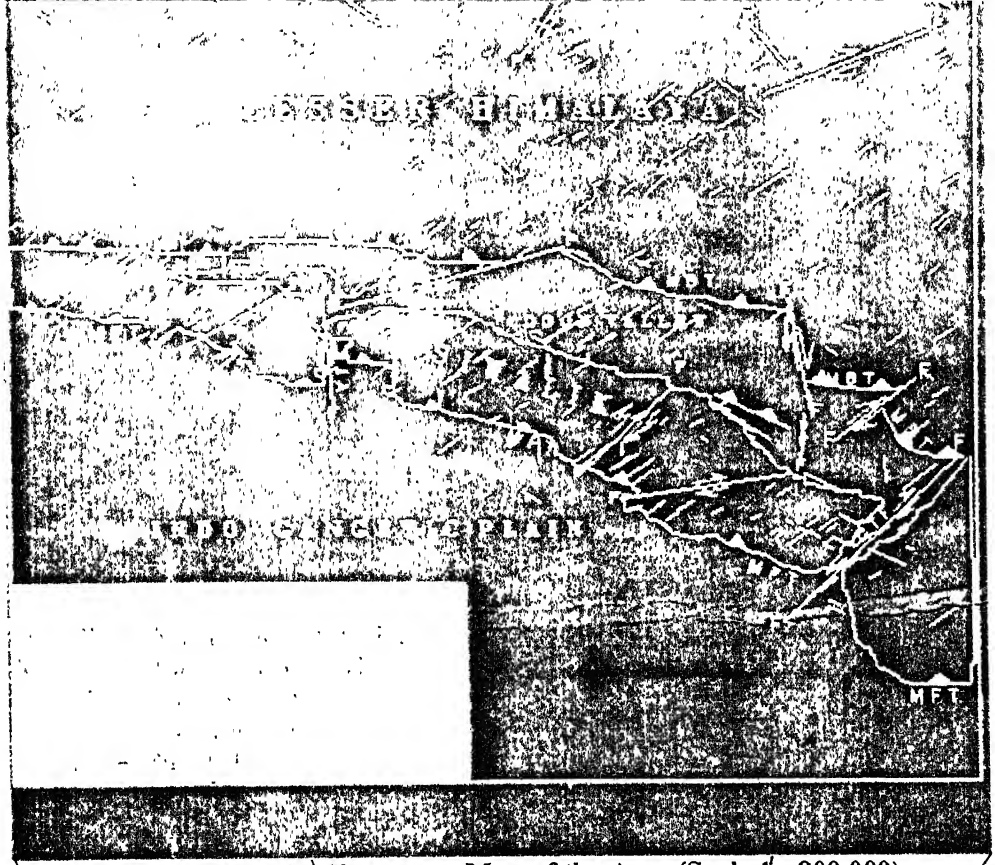

Tectonic - Active lineament Map of the Area (Scale 1 : 800 000)

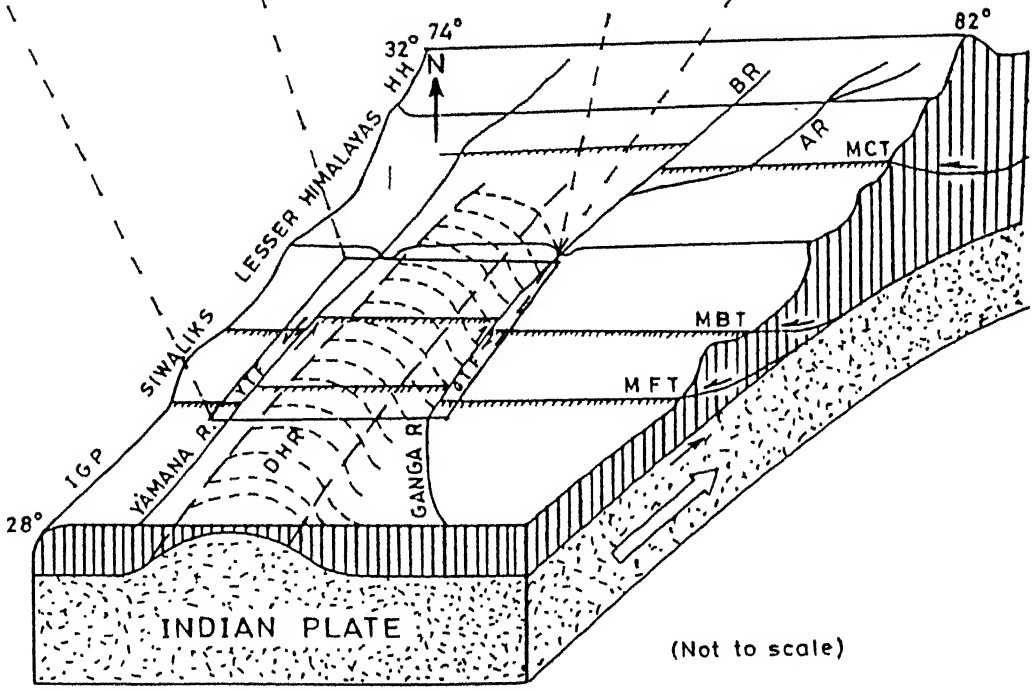

Fig. 4.17 Present day geodynamic framework of the area. IGP : Indo-Gangetic Plain ; HH : Higher Himalaya ; AR : Alaknanda River ; BR : Bhagirathi River ; GTP : Ganga Tear Fault ; YTF : Yamana Tear Fault ; DHR : Delhi - Hardwar Ridge.

CHAPTER V

CONCLUSIONS

In the present work, we have made efforts to integrate remote sensing information, earthquake data and basement data in order to study origin of Ganga and Yamuna tear faults and possible cause of neotectonic activities in the area. From the present work following conclusions have been drawn:

(i) Drainage pattern map of the area has been prepared based on remote sensing data. This map shows that major rivers and streams are highly controlled by joints and faults.

(ii) The analysis of rose diagrams of remotely sensed lineament fabric indicate that the major trend of lineaments in Lesser Himalayan range is almost east-west (N 80^0-90^0 E) and for Dun valley and Siwalik range the trend is NE-SW (N 40^0-50^0 E).

(iii) The orientation of maximum horizontal compressive stress has been found to be about N50^0-60^0 E and N 20^0-30^0 E, in north and south of MBT. It may be due to the anti-clockwise rotation of subducting Indian plate after collision with Eurasian plate.

(iv) Higher density of active faults and lineaments in Siwalik range have been found as compared to the Lesser Himalayan range. The concentration of active lineaments are found to be higher in the intervening zone between Ganga and Yamuna river. This indicates that the region south of MBT is recently more active than north of it.

(v) The active tectonics of the area is controlled in a major way by the subduction of Indian plate with DHR beneath the Siwalik and Lesser Himalayan rocks.

(vi) DHR is an elongated basement ridge starts from Delhi and extends towards north-east direction through Hardwar. Integration of basement depth data and past earthquake data have revealed the seismically active nature of DHR.

(vii) In the study area the flow of Ganga and Yamuna rivers are parallel and are shifting away from each other. This seems to be structurally controlled by DHR.

(viii) The unequal rising and displacement of Siwalik range in north-east direction due to DHR formed the sinistral Yamuna tear fault and dextral Ganga tear fault.

(ix) Relatively more concentration of recently active faults and lineaments in the region between Ganga and Yamuna river are found which can be correlated to the DHR lying below the region.

References

Aditya, S., Raju, A. T. R., (1975), "Assessment of Hydrocarbon Prospect of the sub-Himalayan Panjab and Ganga Basin - India", Geological Survey of India, Misc. Pub. No. 41 (Section III), 127-129.

Cernica, John N., (1995), "Geotechnical Engineering Soil Mechanics", John Wiley and Sons Inc., 259-271.

Dennison, John M., (1968), "Analysis of Geological Structures", Newyork: W. W. Nortron & Company. Inc., First Edition, 1968

Gahalaut, V. K., and Chandra, R., (1992), "On the active tectonics of Dehra Dun region from observation ground level changes", Journal Geological Society of India. Vol.46, 287-294.

Gahalaut, V. K., and Chandra, R., (1995), "Geotechnical and Seismic Risk Implication of Ground Level Changes in the Dehra Dun Region During the 1905-28 period", Journal Geological Society of India, Vol. 46, 287-294.

Gowd, T. N., Sriram Rao, S. V., and Gaur, V. K., (1992), "Tectonic Stress Field in Indian subcontinent", Journal of Geophysical Research, Vol. 97, No. 38, 11,879-11,888.

Gupta, Ravi P., (1991) "Remote Sensing Geology", Springer-Verlag, Germany.

Hock, E., and Bray, J., (1977), "Rock Slope Engineering", The Institution of Mining and Metallurgy, London, 100-101

Lillesand, Thomas M., and Kiefer, Ralph W., (1987), "Remote Sensing and Image Interpretation", John Wiley and Sons, Second Edition.

Mandl, G., (1988), "Mechanics of Tectonic Faulting, Models and Basic Concepts", Elsevier Science Publisher, 11-30.

Murphy, W., (1994), "Remote Sensing Application for Seismic Hazard Assesment", Proceedings of Conference of Royal Society, London, UK entitled "Natural Hazard Assesment and Mitigation: the Unique Role of Remote Sensing", 7-12.

Opdyke, N. D., Johnson, , W. M., Johnson, G. D., Lindsay, E. H., and Tahirkali, R. A. K., 1982, "Paleomagnetism of Middle Siwalik Formation of North Pakistan and Rotation of Salt Range Decollement", Journal of Paleontological Research, Vol. 67, 1-15.

Philip, G., (1996), "Landsat Thematic Mapper Data Analysis for quaternary tectonics in parts of the Doon Valley, NW Himalaya, India", International Journal of Remote Sensing, Vol.17, No.1, 143-153.

Project Report on Environmental Impact Assesment and Environmental Management Plan of Manal Limestone Quarry (Rajban, H.P), 1992, sponsored by C. C. I. L., New Delhi; Submitted by Department of Earth Sciences, University of Roorkee, Roorkee.

Qureshy, M. N., and Hinze,W., J., (1989), "Geophysical Lineaments their tectonic and Economic Significance", Memoir of Geological Society of India, No. 12, 2-5.

Qureshy, M. N., and Kumar, S., (1992), "Isostasy and Neotectonics of NW Himalaya and Foredeep", Memoir Geological Society of India, No. 23, 201-222.

Rautela, P., and Sati, D., (1996), "Recent Crustal Adjustments in Dehra Dun valley , Western U. P., India", Current Science, Vol.71, No. 10, 776-780,

Raval, U., (1995), "On a Geodynamical Visualization of Uttarkashi Earthquake and its Generalization", Memoir of Geological Society of India, No. 30, 203-224.

Richard, John A., (1993), "Remote Sensing Digital Image Processing: An Introduction", Springer-Verlag, Second Edition.

Roy, B. C., and Hasija, N. L., (1995), "Coseismic and Post Seismic Crustal Deformation in the Doon valley as Determined From Repeat levelling", Memoir of Geological Society of India, No. 30, 173-178.

Roy, B. C., and Hasija, N. L., (1995), "Geodetic Evidence of Preseismic Tectonic Activity in Garhwal Himalaya", Memoir of Geological Society of India, No. 30, 179-190.

Thornbury, W. D., (1989), "Principle of Geomorphology", Wiley Eastern Limited, Second Edition, 117-127.

Valdiya, K. S., 1980, Stratigraphic scheme of the sedimentary units of the Kummaon lesser Himalaya Formation, Hindustan Publishing Corp. (India), Delhi, 7-48.

Valdiya, K. S., 1986, "Neotectonic activities in the Himalayan belt, Proceedings of International Symposium on Neotetonics in Soth Asia. (Dehra Dun: Survey of India), 241-251.

Verma, R. K., Roonwal, G. S., Kamble, V. P., Dutta, U., Kumar, N., Gupta, Y., and Sood, S., (1995), " Seismicity of Northwestern part of the Himalayan Arc, Delhi Hardwar Ridge and Garhwal-Kumaun Himalayan Region, A synthesis of existing data", Memoir of Geological Society of India", No. 30, 83-99.

Walter, Louis S., (1994), "Natural Hazard Assesment and Mitigation from Space: The Potential of Remote Sensing to meet Operational Requirement", Proceedings of conference of Royal Society, London, UK entitled "Natural Hazard Assesment and Mitigation: The Unique Role of Remote Sensing", 7-12.

APPENDIX I

COMPUTER PROGRAM

```
/*****************************************************************/
/* Author: Pradeep K. Sahoo                                      */
/* Date: 07/05/1997                                              */
/* Input: A digitize file (.DIG file) created in ERDAS           */
/*Outputs:                                                       */
/*1. Input data to plot Rose diagram of lineament data          */
/*2. Input data to plot stress Rose diagram                     */
/*3. Active lineament generation in ERDAS file format (.DIG file) */
/*****************************************************************/
#include <stdio.h>
#include <math.h>
#include <ctype.h>
#include <string.h>
#define MAXLINE 200
/* MAXLINE: maximum length of a line in the input DIG file       */


/*****************************************************************/
/* Function declaration                                          */
getline(line);
makedata( );
/*****************************************************************/
FILE *fpdig, *fpline, *fpstress, *fpactive;
char filedig[20], fileline[20], filestress[20], fileactive[20];
main( )
```

```
{
char line[MAXLINE];
int j;
printf ("Enter the input DIG file name\n");
scanf ("%s", filedig);
printf ("Enter the output lineament file name(.dat)\n");
scanf("%s",fileline);
printf("Enter stress file name (.dat)\n");
scanf("%s", filestress);
printf("Enter the Active lineament file name(.DIG)\n");
scanf("%s", fileactive);
if ((fpdig = (fopen(filedig, "r"))) = = NULL)
{
  printf("File %s dose not exit\n", fpdig);
   exit(1);
}
fpactive = fopen (fileactive, "w");
fp = fopen ("temp", "w");
/* Copy the first five lines of the input dig file to active lineament file
        */
for (j=1; j<=5; j++)
{
  getline(line);
fprintf(fpactive, "%s", line);
}
/* Copy the latitude and longitude data in a temporary file temp
for (j=1; j<=300; j++)
```

```
{
  getline(line);
  if ((j%3) != 1)
    fprintff (fp, "%s", line);
}
makedata( );
}
/*************************************************************************/
getline(line)
/*The function getline(line) reads a line from the input dig file and stores it in the array
line[ ]*/
/*The semicolon at the end of each line of the input DIG file is not read          */
char line[ ]
{
  int c, i;
  for (i=0; i<MAXLINE; i++)
  line [i] = ' ';
   for (i=0; i<MAXLINE-1 && (c = fgetc(fpdig)) != EOF && c != '\n'; i++)
       if (c != ';' ) line [i] = c;
   if (c = = '\n')
    {
       LINE [i] = c;
        ++i;
     }
   line[i] = '\0';
}
/*************************************************************************/
```

```
makedata( )
{
float pi = 3.141592654;
float x1,x2,y1,y2,data1,data2,data3,data4;
float theta, angle, phi, alpha, beta, dummy;
float minx1, maxx1, miny1, maxy1, mixs, maxxs, minys, maxys;
int interv=10, i, j, freqline[50], freqstress[50];
int sum = 0;

for (i=0; i<50; i++)
  freqline[i] = 0;
for (i=0; i<50; i++)
  freqstress[i] = 0;

printf("Enter the value of phi (degrees):      ");
scanf("%f", &phi);
phi = phi*pi/180.0;

alpha = pi/4 - phi/2;

fclose(fp);
fp = fopen (fileline, "w");
fpstress = fopen(filestress, "w");
while (!feof(fp))
{
   fscanf (fp, "%f %f %f %f", &x1,&y1,&x2,&y2);
    theta = atan2 (y2-y1, x2-x1);
```

```
if (theta < 0)
   theta += pi;
if ((theat >=0) && (theta <= pi/2))
  beta = theat + alpha;
else
    beta = theat - alpha;
dumy = beta *180/pi;
if (((dumy >= 60) && (dummy <= 70)) !! ((dumy >= 110) && (dummy <=1300)))
{
   printf("beta = %f\n", beta*180/pi);
    fprintf(fpactive, "   -2          1          100       2          ;\n");
    fprintf(fpactive, "    %f       %f;\n", x1, y1);
    ffprintf(fpactive, "    %f       %f,\n", x2,y2);
}
```

APPENDIX II

APPROPRIATE VALUES FOR THE BASIC FRICTIONAL ANGLE ϕ FOR DIFFERENT ROCKS.

Rocks	ϕ (degree angle)
Amphibolite	32
Basalt	31-38
Conglomerate	35
Chalk	30
Dolomite	27-31
Gneiss (Schist)	23-29
Granite (fine grained)	29-35
Granite (coarse grained)	21-35
Limestone	33-40
Porphyry	31
Sandstone	25-35
Shale	27
Siltstone	27-31
Slate	25-30

(Source: Hock and Bray, 1977)